JBC RESEARCH ARTICLE

The BCKDK inhibitor BT2 is a chemical uncoupler that lowers mitochondrial ROS production and *de novo* lipogenesis

Received for publication, August 15, 2023, and in revised form, January 12, 2024 Published, Papers in Press, January 30, 2024,
https://doi.org/10.1016/j.jbc.2024.105702

Aracely Acevedo[1], Anthony E. Jones[1], Bezawit T. Danna[1], Rory Turner[2], Katrina P. Montales[3], Cristiane Benincá[3], Karen Reue[4], Orian S. Shirihai[3], Linsey Stiles[3], Martina Wallace[2], Yibin Wang[5], Ambre M. Bertholet[6], and Ajit S. Divakaruni[1,*]

From the [1] Department of Molecular and Medical Pharmacology, University of California, Los Angeles, Los Angeles, California, USA; [2]School of Agriculture and Food Science, University College Dublin, Dublin, Ireland; [3]Department of Medicine, and [4]Department of Human Genetics, University of California, Los Angeles, Los Angeles, California, USA; [5]DukeNUS School of Medicine, Signature Research Program in Cardiovascular and Metabolic Diseases, Singapore, Singapore; [6]Department of Physiology, University of California, Los Angeles, Los Angeles, California, USA

Reviewed by members of the JBC Editorial Board. Edited by Clare E. Bryant

Elevated levels of branched chain amino acids (BCAAs) and branched-chain α-ketoacids are associated with cardiovascular and metabolic disease, but the molecular mechanisms underlying a putative causal relationship remain unclear. The branched-chain ketoacid dehydrogenase kinase (BCKDK) inhibitor BT2 (3,6-dichlorobenzo[b]thiophene-2-carboxylic acid) is often used in preclinical models to increase BCAA oxidation and restore steady-state BCAA and branched-chain α-ketoacid levels. BT2 administration is protective in various rodent models of heart failure and metabolic disease, but confoundingly, targeted ablation of *Bckdk* in specific tissues does not reproduce the beneficial effects conferred by pharmacologic inhibition. Here, we demonstrate that BT2, a lipophilic weak acid, can act as a mitochondrial uncoupler. Measurements of oxygen consumption, mitochondrial membrane potential, and patch-clamp electrophysiology show that BT2 increases proton conductance across the mitochondrial inner membrane independently of its inhibitory effect on BCKDK. BT2 is roughly sixfold less potent than the prototypical uncoupler 2,4-dinitrophenol and phenocopies 2,4-dinitrophenol in lowering *de novo* lipogenesis and mitochondrial superoxide production. The data suggest that the therapeutic efficacy of BT2 may be attributable to the well-documented effects of mitochondrial uncoupling in alleviating cardiovascular and metabolic disease.

Elevations in circulating levels of the branched-chain amino acids (BCAAs), leucine, isoleucine, and valine, are a hallmark of metabolic and cardiovascular disease (1–5). Early studies dating back over 50 years showed that elevated blood levels of BCAAs positively correlated with obesity and blood insulin levels in patients relative to matched lean individuals (6). Further studies leveraging unbiased metabolomics have reinforced the links between BCAA accumulation and insulin resistance in both humans and preclinical rodent disease models (7, 8). In fact, longitudinal studies tracking healthy individuals showed that elevated plasma BCAAs could be predictive of future insulin resistance (8, 9).

As with obesity and insulin resistance, epidemiological studies have also linked elevated circulating levels of both BCAAs and their breakdown products, branched-chain α-ketoacids (BCKAs), with cardiovascular disease. In both humans and rodents, several studies point to accumulation of BCAAs and/or BCKAs in heart failure, myocardial infarction (MI) and ischemia, hypertension, and arrhythmia (1, 10–14). Furthermore, elevated plasma BCAAs may be predictive of future obstructive coronary artery disease (15).

Steady-state levels of BCAAs are a balance of intake and disposal. BCAAs are essential amino acids for humans and animals, meaning they cannot be synthesized *de novo*. Dietary intake is therefore the predominant source of BCAAs, though a minor proportion may arise from the gut microbiome (4). Along with protein synthesis, BCAA oxidation represents an important sink for clearing BCAAs and maintaining homeostatic levels (4, 5).

Oxidation of leucine, isoleucine, and valine is a tightly regulated process. Each BCAA is first deaminated by the branched-chain aminotransferase to its respective BCKA. These BCKAs then undergo irreversible decarboxylation and esterification to their respective R-CoA molecules by the branched-chain α-ketoacid dehydrogenase (BCKDH). They are eventually incorporated into the tricarboxylic acid (TCA) cycle as acetyl CoA or succinyl CoA. Much like regulation of the pyruvate dehydrogenase by inhibitory kinases and an activating phosphatase, the BCKDH is inhibited by the BCKDH kinase (BCKDK) and activated by the mitochondrial protein phosphatase 2Cm (PP2Cm) (16, 17).

The association between increased BCAA and BCKA levels and cardiovascular and metabolic disease is well accepted, but it remains unclear whether these elevated levels have a causative role in disease or represent an indirect epiphenomenon. Several proof-of-concept studies have sought to modify BCAA intake in preclinical models to examine how readjusting steady-state levels affects disease pathology. As it relates to insulin resistance, dietary BCAA supplementation has

* For correspondence: Ajit S. Divakaruni, adivakaruni@mednet.ucla.edu.

produced mixed results suggesting a complex and contextual effect dependent on the composition of diet and pre-existing health of the animal (4, 7). Dietary restriction of BCAAs, however, reverses insulin resistance in multiple preclinical studies (7, 18). Although fewer studies are available examining dietary BCAAs on cardiovascular disease, one report noted that oral BCAA administration post-MI impaired contractility and increased infarct size (19).

Numerous studies have manipulated metabolic enzymes to alter steady-state BCAA and BCKA levels and examined the disease-modifying impact. Indeed, whole-body deletion or silencing of the PP2Cm increases circulating BCAA levels and promotes heart failure and worsens ischemia/reperfusion (I/R) injury (12, 20). In line with these results, tissue-specific adenoviral overexpression of this phosphatase lowered BCKA and BCAA levels and prevented ischemic injury in the heart (21) and reduced hepatic triglyceride accumulation and improved hepatic glucose tolerance (22).

Some of the strongest evidence for a causative and pathological relationship between dysregulated BCAA metabolism and cardiometabolic disease comes from pharmacologic inhibition of the BCKDK with BT2 (3,6-dichlorobenzo[b]thiophene-2-carboxylic acid). The small molecule BT2 was designed as a BCKA analog that allosterically binds to the BCKDK (23). Similar to end-product inhibition of BCKDK by elevated BCKA levels, the compound relieves kinase inhibition on the BCKDH and promotes BCKA oxidation. In preclinical models of heart failure, systemic BT2 administration lowers cardiac BCAAs and BCKAs and provides cardioprotection in response to both transaortic constriction as well as left anterior descending artery ligation (12, 19–21). In various rodent models of cardiometabolic disease, BT2 lowers circulating BCAA and BCKAs, improves glucose tolerance and insulin sensitivity, and reduces *de novo* lipogenesis (DNL) (22, 24–26).

Remarkably, however, the recent development of tissue-specific mouse models has complicated our understanding of how dysregulated BCAA metabolism may relate to cardiovascular and metabolic disease. Cardiac-specific loss of BCKDK does not reproduce the protective effects in either hemodynamic models or ischemic models of heart failure (27). It could be argued that the proportion of BCAA oxidation in the heart is too low for the cardiac-specific knockout to have an effect on circulating BCAA levels similar to BT2 (28). However, inducible skeletal muscle–specific *Bckdk* ablation also failed to elicit cardioprotection despite lowering cardiac BCAAs and plasma BCAAs and BCKAs (27). Furthermore, tissue-specific loss of BCKDK in skeletal muscle does not reproduce the effects of BT2 in improving insulin sensitivity despite lowering plasma BCAAs and BCKAs (29). Similar loss-of-function studies show that hepatic BCKDK loss also fails to improve insulin sensitivity (26, 29), though the liver has less apparent control over circulating BCAA levels than muscle. While the results could suggest that whole-body BCKDK inhibition cannot be reproduced by *Bckdk* ablation in individual tissues, they perhaps also suggest an alternative mechanism by which BT2 confers protection from heart failure and metabolic disease distinct from BCAA oxidation.

Here, we present evidence that BT2 is a mitochondrial uncoupler. Measurements of respiration, mitochondrial membrane potential, and inner membrane electrophysiology all demonstrate that BT2—a lipophilic weak acid—is itself a chemical uncoupler. BT2 also phenocopies the prototypical uncoupler 2,4-dinitrophenol (DNP) in lowering mitochondrial hydrogen peroxide (H_2O_2) efflux and reducing DNL. Chemical uncoupling of mitochondria provides a single and parsimonious mechanism by which BT2 could plausibly confer protection against heart failure (lowering mitochondrial reactive oxygen species [ROS] production) and cardiometabolic disease (increasing energy expenditure) independent of effects on steady-state BCAA levels.

Results

BT2 uncouples mitochondria in rodent and human cardiomyocytes

To identify uncharacterized metabolic targets or mechanisms of BT2 action independent of its inhibitory effect on the BCKDK, we measured the effect of BT2 on the oxygen consumption rate in neonatal rat ventricular myocytes (NRVMs). Acute BT2 administration 5 min prior to initial measurements revealed a consistent increase in the basal respiration rate (Fig. 1, *A* and *B*). This increase persisted in the presence of the ATP synthase inhibitor oligomycin, but no change was observed when measuring the maximal respiratory capacity with FCCP (carbonyl cyanide 4-trifluoromethoxyphenylhydrazine). The result mimics the hallmark profile of mitochondrial uncoupling (30, 31): BT2 increased mitochondrial oxygen consumption independently of (or "uncoupled" from) ATP synthesis. Indeed, the uncoupling response was preserved when cardiomyocytes were stimulated with norepinephrine (Fig. 1*B*) and was observed at concentrations as low as 5 μM (Fig. 1*C*). Moreover, acute BT2 administration also increased respiration associated with proton leak in iCell human-induced pluripotent stem cell (iPSC)–derived cardiomyocytes, with and without adrenergic activation (Fig. 1*D*). Given that BT2 acutely increases oligomycin-insensitive respiration in human and rodent cardiomyocytes, we hypothesized that it can act as a chemical uncoupler.

Chemical uncouplers such as FCCP or DNP increase the oxygen consumption rate because they stimulate consumption of the mitochondrial membrane potential independently of ATP synthesis, thereby causing increased activity of the respiratory chain (31). We therefore measured the resting mitochondrial membrane potential in iCell cardiomyocytes and NRVMs in response to acute treatment with BT2 (Fig. 1, *E* and *F*). In both model systems, fluorescence of the lipophilic cation dye TMRE (tetramethylrhodamine, ethyl ester) showed a ∼10% decrease in the steady-state membrane potential with little change to mitochondrial morphology in response to BT2. This result could be reproduced by the classic uncoupler DNP. Moreover, the changes observed with BT2 and DNP were qualitatively, but not quantitatively, matched by the extreme changes in membrane potential observed from the highly potent uncoupler FCCP. The demonstration that BT2 slightly

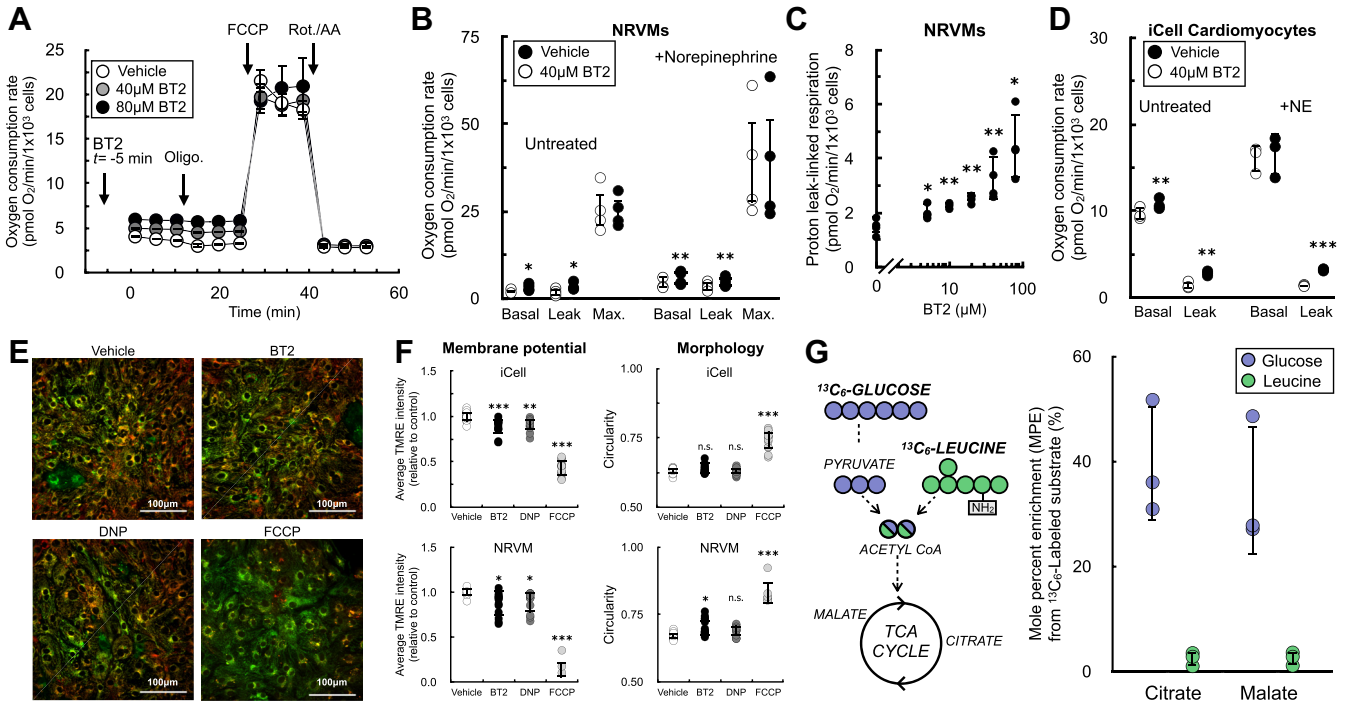

Figure 1. BT2 acutely uncouples mitochondria in rat and human cardiomyocytes. *A*, representative oxygen consumption trace of neonatal rat ventricular myocytes (NRVMs) offered 40 μM BT2, 80 μM BT2, or vehicle control (DMSO) 5 min prior to conducting measurements. Forty micro molars and eighty micro molars BT2 were chosen as concentrations because they are 10-fold above the EC_{50} (40 μM) or previously used in the literature (80 μM) (84). (n = 10 technical replicates from a single experiment). *B*, collated oxygen consumption rate parameters for NRVMs offered 40 μM BT2 in the presence or the absence of 1 μM norepinephrine. (n = 4 biological replicates). *C*, proton leak–linked respiration in NRVMs. Experiments conducted as in (*A* and *B*). [BT2] = 5, 10, 20, 40, and 80 μM. (n = 4 biological replicates). *D*, collated oxygen consumption rate parameters for human iPSC-derived iCell cardiomyocytes offered 40 μM BT2 in the presence or the absence of 1 μM norepinephrine as in (*B*). (n = 4 biological replicates). *E*, representative images for iCell cardiomyocytes treated for 20 to 40 min with 80 μM BT2, 10 μM DNP, 1 μM FCCP, or vehicle control. Ten nano molars TMRE and two hundred nano molars MitoTracker Green FM were given 1 h to equilibrate prior to compound addition (further details available in the Experimental procedures section). *F*, *left*, average TMRE intensity relative to vehicle control for treatments as in (*D*) with iCell cardiomyocytes (*top*) and NRVMs (*bottom*). *Right*, circularity as a measure of mitochondrial morphology for treatments as in (*D*) with iCell cardiomyocytes (*top*) and NRVMs (*bottom*). (n = 7–15 technical replicates collated from n = 3 biological replicates for each cell type). *G*, *left*, simplified schematic of uniformly labeled $^{13}C_6$-glucose or $^{13}C_6$-leucine enriching TCA cycle intermediates. *Right*, mole percent enrichment (M.P.E.) of TCA cycle intermediates citrate and malate in NRVMs with the ^{13}C label provided on either glucose or leucine. (n = 3 biological replicates). *Panels* (*B–D*, and *G*) show data as mean ± SD of individual biological replicates. Panels (*A* and *F*) show data as mean ± SD from technical replicates. Statistical analysis was conducted with a pairwise Student's *t* test {[(*B* and *C*), each BT2 concentration against vehicle control], and (*D*)} or ANOVA followed by Dunnett's posthoc multiple comparison tests (*E*) as appropriate. *$p < 0.05$; **$p < 0.01$; and ***$p < 0.001$. BT2, 3,6-dichlorobenzo[b] thiophene-2-carboxylic acid; DMSO, dimethyl sulfoxide; DNP, 2,4-dinitrophenol; FCCP, carbonyl cyanide 4-trifluoromethoxyphenylhydrazine; iPSC, induced pluripotent stem cell; TCA, tricarboxylic acid; TMRE, tetramethylrhodamine, ethyl ester.

lowers the steady-state membrane potential similarly to DNP aligns with the oxygen consumption results and supports the hypothesis that BT2 can act as a chemical uncoupler.

We further sought to determine whether our *in vitro* cardiomyocyte models behaved similarly to recent *in vivo* human and rodent studies that show or infer little BCAA oxidation in the heart relative to other substrates (27, 28). We offered NRVMs medium with a uniform $^{13}C_6$ label on either glucose or leucine to measure relative incorporation of each substrate into the TCA cycle (Fig. 1*G*). Incorporation of labeled leucine into the TCA cycle intermediates citrate and malate was more than 10-fold lower than incorporation of labeled glucose. Furthermore, BT2 stimulated uncoupled respiration in a range of cultured cell lines, including those that lacked measurable incorporation of labeled leucine into TCA cycle intermediates (Fig. S1). Altogether, the demonstration that BT2 could uncouple respiration in cells with marginal rates of BCAA oxidation—in addition to the acute time frame in which BT2 increases in proton leak–associated respiration—suggested a mechanism independent of BCKDK inhibition. As such, we sought to confirm this by using reductionist systems where specific metabolic pathways and reactions could be isolated.

BT2 is a chemical uncoupler

To formally rule out the involvement of BCKDK activity in the uncoupling phenotype observed in rat and human cardiomyocytes, we measured the acute effects of the compound on isolated mitochondria. Isolated mitochondria are a well-defined system that can be used to isolate specific metabolic reactions and pathways (30, 32). We first measured respiration in mitochondria offered specific substrates to isolate the effects of BT2 on targeted metabolic pathways that bypass the BCKDK. In isolated liver mitochondria offered pyruvate and malate, acute BT2 treatment 5 min prior to measurements elicited a similar and specific effect on mitochondrial uncoupling as we had observed in intact cells. BT2 caused a concentration-dependent increase in respiration associated

with proton leak ("state 4_o"), but no change was observed in ADP-stimulated ("state 3") or FCCP-stimulated ("state 3_u") respiration (Fig. 2, *A* and *B*). In liver mitochondria isolated from both rat and mouse, BT2 showed a similar concentration-dependent increase in state 4_o respiration irrespective of whether the mitochondria were provided pyruvate, glutamate, or succinate as a respiratory substrate (Fig. 2*C*). Depending on the substrate and species, an increase in proton leak–associated respiration was observed at BT2 concentrations as low as 2.5 μM. In mitochondria isolated from rat and mouse hearts, BT2 also acutely increased state 4_o respiration independent of the substrate provided to the mitochondria

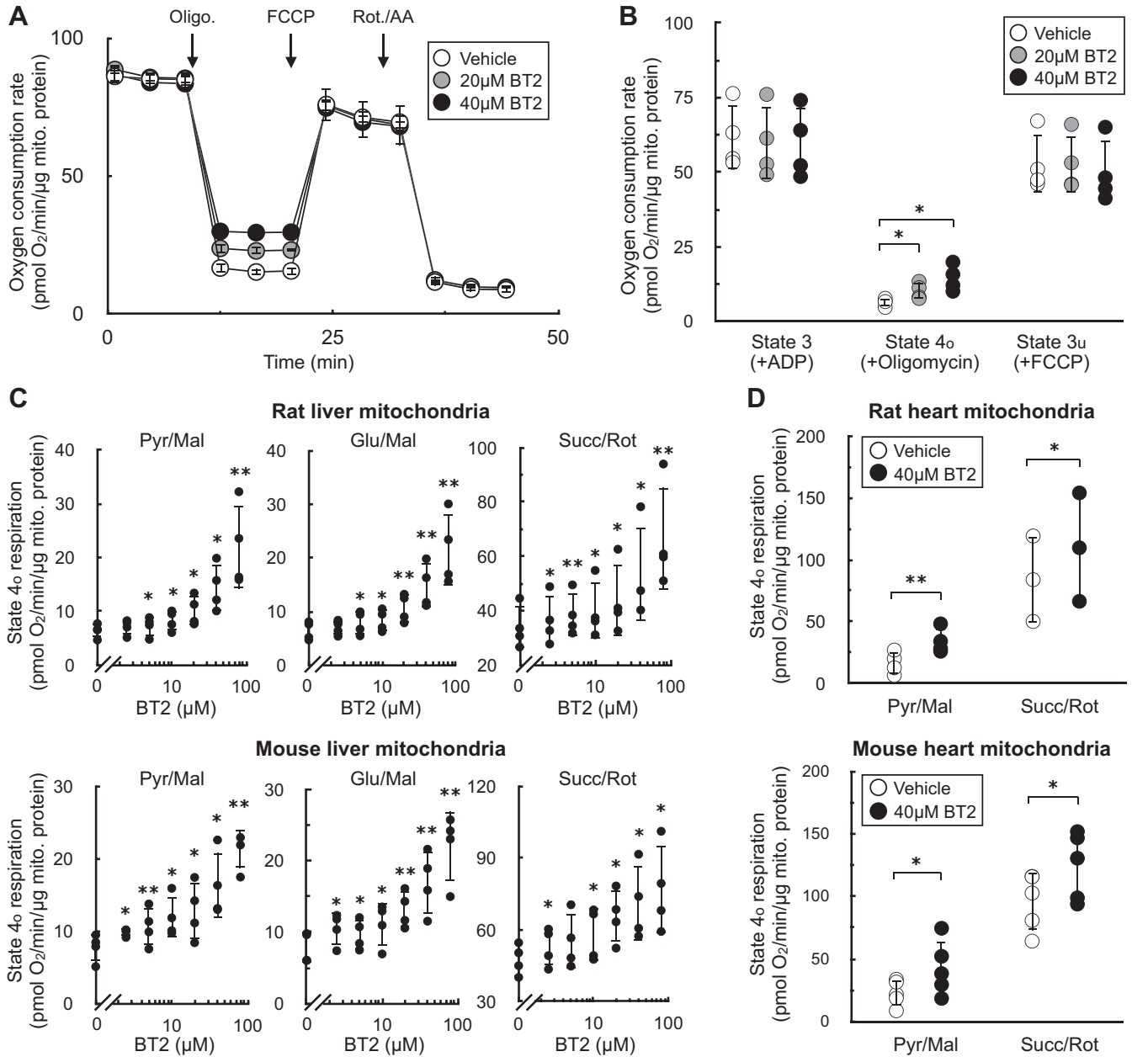

Figure 2. BT2 increases state 4_o respiration in isolated mitochondria. *A*, representative oxygen consumption trace of isolated liver mitochondria acutely treated with vehicle control, 20 μM BT2, or 40 μM BT2 5 min prior to initial measurements. Mitochondria were offered pyruvate, malate, and ADP in the experimental medium, and respiration was measured in response to sequential injections of oligomycin, FCCP, and rotenone with antimycin A. (n = 5 technical replicates from a single experiment). *B*, collated oxygen consumption rate parameters for isolated liver mitochondria as in (*A*). (n = 4 biological replicates). *C*, state 4_o respiration in isolated mitochondria from rat liver (*top*) or mouse liver (*bottom*). Experiments conducted as in (*A*) with pyruvate/malate (*left*), glutamate/malate (*middle*), or succinate/rotenone (*right*) offered as respiratory substrates. [BT2] = 2.5, 5, 10, 20, 40, and 80 μM. (n = 4 biological replicates). *D*, state 4_o respiration in isolated mitochondria from rat heart (*top*) or mouse heart (*bottom*) acutely offered either vehicle control (DMSO) or 40 μM BT2 5 min prior to initial measurements. Experiments conducted as in (*A*) with either pyruvate/malate (*left*) or succinate/rotenone (*right*) offered as respiratory substrates. Panels (*B–D*) show data as mean ± SD of individual biological replicates. *A*, shows data as mean ± SD from technical replicates. Statistical analysis was conducted with a pairwise Student's *t* test {[(*C*), each BT2 concentration against vehicle control] or (*D*)} or ANOVA followed by Dunnett's posthoc multiple comparison tests (*B*) as appropriate. *$p < 0.05$; **$p < 0.01$. BT2, 3,6-dichlorobenzo[b]thiophene-2-carboxylic acid; DMSO, dimethyl sulfoxide; FCCP, carbonyl cyanide 4-trifluoromethoxyphenylhydrazine.

(Fig. 2*D*). In total, respiration with isolated mitochondria showed that BT2 can uncouple isolated mitochondria at single-digit micromolar concentrations regardless of the respiratory substrate provided.

As in Figure 1, we sought to corroborate our oxygen consumption results with measurements of the mitochondrial membrane potential. We therefore examined whether acute BT2 administration would lower the membrane potential in isolated mitochondria by measuring the loss of quenched TMRE fluorescence (33). The approach was validated by examining the acute effects of oligomycin and FCCP: ATP synthase inhibition by oligomycin increased the membrane potential and further quenched the TMRE signal, whereas the potent uncoupler FCCP caused a substantial loss of the quenched fluorescence (Fig. 3*A*). As expected, acute BT2 treatment lowered the quenched fluorescence of TMRE in both heart and liver mitochondria, indicating a reduced membrane potential and further suggesting that the compound itself is a chemical uncoupler (Fig. 3*B*).

The acute increase in state 4_o respiration (Fig. 2) and decrease in membrane potential in isolated mitochondria strongly infer that BT2 increases proton conductance across the inner mitochondrial membrane (IMM) (31). However, a definitive and unassailable measure of mitochondrial uncoupling requires direct measurement of the proton current. We therefore conducted patch-clamp electrophysiological measurements of the inner membrane in mitoplasts derived from isolated heart mitochondria (34). Indeed, a measurable increase in proton current could be observed across the inner membrane in response to BT2 (Fig. 3, *C* and *D*). Taken together, results from respirometry, TMRE fluorescence, and membrane electrophysiology all point to a chemical uncoupling property of BT2 independent of its effects on BCAA metabolism.

BT2 is approximately sixfold less potent than DNP

With clear evidence that BT2 can act as a chemical uncoupler, we then sought to gauge its potency in relation to the other well-known uncouplers DNP, FCCP, and Bam15. Similar

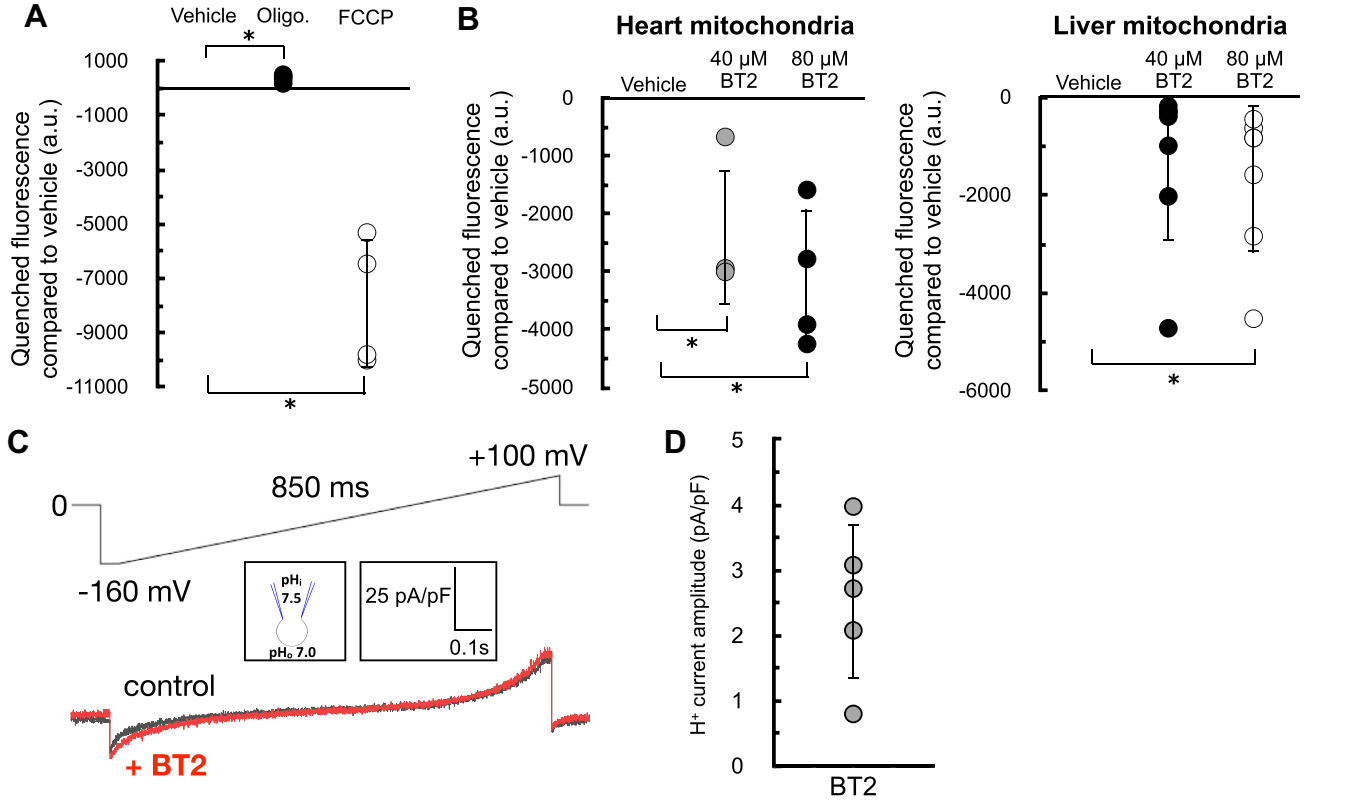

Figure 3. BT2 lowers membrane potential in isolated mitochondria and increases proton conductance across the mitochondrial inner membrane. *A*, quenched TMRE fluorescence in isolated rat liver mitochondria offered succinate, rotenone, and ADP as described in the Experimental procedures section. Mitochondria were offered oligomycin (1 µg/mg mitochondrial protein) or FCCP (1 µM) 5 min prior to measurements as controls to demonstrate the signal responds appropriately to known effector compounds. (n = 3 biological replicates). *B*, quenched TMRE fluorescence as in (*A*) in response to 40 µM BT2, 80 µM BT2, or vehicle controls in isolated rat heart (*left*) or rat liver (*right*) mitochondria. (n = 4 biological replicates). *C*, representative current induced by 100 µM BT2 recorded from heart mitoplasts. Traces are shown before (control, *black*) and after (*red*) the addition of BT2 to the bath solution. The voltage protocol is indicated above the trace. Bath (cytosolic side of the inner mitochondrial membrane) and pipette (matrix side) pH are indicated in the pipette–mitoplast diagram. *D*, aggregate current densities at −160 mV from the protocol described in (*C*). BT2-dependent currents correspond to the difference between the control current and that in the presence of BT2. Currents were normalized per membrane capacitance to obtain current densities (pA/pF). (n = 5 biological replicates). All data are shown as mean ± SD of individual biological replicates. Statistical analysis was conducted with ANOVA followed by Dunnett's posthoc multiple comparisons tests. *$p < 0.05$. BT2, 3,6-dichlorobenzo[b]thiophene-2-carboxylic acid; FCCP, carbonyl cyanide 4-trifluoromethoxyphenylhydrazine; TMRE, tetramethylrhodamine, ethyl ester.

to these chemical uncouplers, BT2 is lipophilic and contains a functional group that can reversibly dissociate with a proton (Fig. 4*A*). We therefore sought to quantify the potency of BT2 by measuring its concentration-response curve for state 4_o respiration alongside other chemical uncouplers in isolated liver mitochondria (Fig. 4, *B* and *C*). Similar to DNP, BT2 is a far less potent uncoupler than either FCCP or Bam15 and requires $>10^3$-fold more compound to elicit a similar change in proton leak–linked respiration (Fig. 4*D*). Relative to DNP, roughly six times the concentration of BT2 is required to elicit the same change in respiration in mitochondria isolated from both rat liver (Fig. 4*D*) and heart (Fig. 4*E*). Single-point measurements of quenched TMRE fluorescence also show a similar potency profile for BT2 relative to other uncouplers (Fig. 4*F*), as more BT2 is required to drop the mitochondrial membrane potential to a similar degree relative to other chemical uncouplers. Encouragingly, quantitative comparison of the proton current amplitude (pA/pF) elicited from 100 μM BT2 in electrophysiological studies (Fig. 3*D*) is broadly sixfold lower than that from previous measurements of 100 μM DNP (BT2: 2.52 ± 0.53 [SEM; n = 5]; DNP: 15.82 ± 1.28 [SEM; n = 9] (35)). Higher concentrations of BT2 disrupted the integrity of the inner membrane such that proton currents could not be reliably quantified, precluding multipoint comparisons between BT2 and DNP (Fig. S2). Altogether, respiration and membrane potential measurements in isolated mitochondria show BT2 is three orders of magnitude less potent than Bam15 and FCCP and about sixfold milder than the well-studied and prototypical uncoupler DNP.

BT2 uncouples via *both ADP/ATP carrier–dependent and ADP/ATP carrier–independent mechanisms*

Chemical uncouplers have at least two distinct mechanisms: (i) a conventional model whereby weak acid/anion cycling across the IMM dissipates the proton gradient across the inner membrane (36) and (ii) stimulating proton conductance through the ADP/ATP carrier (AAC) by binding to the nucleotide translocation site (35, 37, 38). As such, we sought to determine whether BT2 also uncoupled *via* both AAC-dependent and AAC-independent mechanisms to provide further evidence that it is a conventional chemical uncoupler. We employed both pharmacologic and genetic strategies to inhibit AAC activity and measure BT2-stimulated increases in state 4_o respiration. In isolated rat liver mitochondria, inhibition of adenine nucleotide translocation with carboxyatractyloside had a predictable effect of inhibiting ADP-stimulated respiration similarly to oligomycin (Fig. 5*A*). Quantifying the increase in state 4_o respiration from BT2 in the presence and the absence of carboxyatractyloside showed

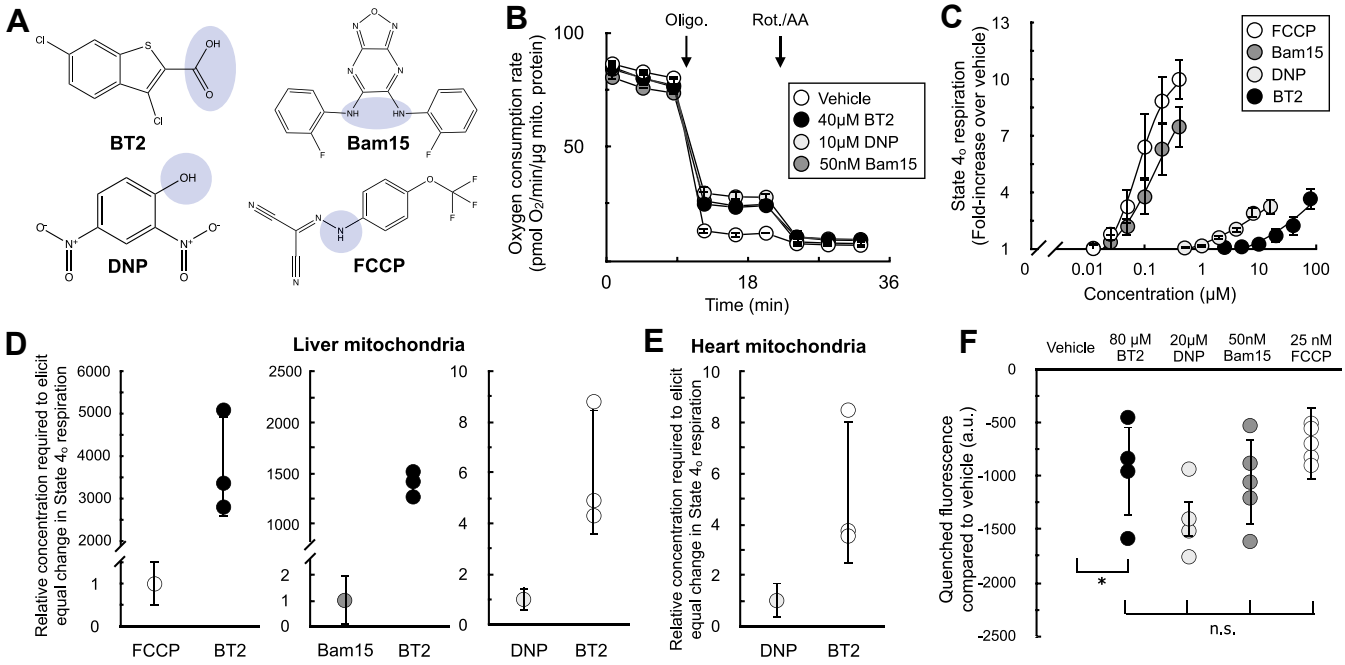

Figure 4. BT2 is a less potent chemical uncoupler than FCCP, Bam15, and DNP. *A*, chemical structures of BT2, DNP, Bam15, and FCCP with the functional group for weak acid/anion cycling highlighted in *blue*. *B*, representative trace of isolated liver mitochondria acutely offered 40 μM BT2, 10 μM DNP, or 50 nM Bam15. Assay medium is supplemented with pyruvate, malate, and ADP as before. (n = 4 technical replicates from a single experiment). *C*, aggregate fold change in state 4_o respiration relative to vehicle controls from experiments conducted as in (*B*). [FCCP] and [Bam15] = 400, 200, 100, 50, 25 nM; [DNP] = 16, 8, 4, 2, 1, 500 nM; [BT2] = 2.5, 5, 10, 20, 40, and 80 μM. (n = 4 biological replicates). *D*, data extrapolated from experiments conducted in (*A* and *B*) measuring difference in concentration required to elicit a twofold and threefold change in the state 4_o rate relative to vehicle controls. (n = 4 biological replicates). *E*, values calculated as in (*A*)–(*C*) except with isolated rat heart mitochondria. (n = 4 biological replicates). *F*, mitochondrial membrane potential measurements using quenched TMRE fluorescence with isolated liver mitochondria as in Figure 2, *A*–*C*. (n = 4 biological replicates). Panels (*C*–*F*) show data as mean ± SD of individual biological replicates. The means are presented for panel (*C*) rather than individual data points for clarity. Panel (*B*) shows data as mean ± SD from technical replicates. Statistical analysis was conducted with ANOVA followed by Dunnett's posthoc multiple comparisons tests (*F*). *$p < 0.05$. BT2, 3,6-dichlorobenzo[b]thiophene-2-carboxylic acid; DNP, 2,4-dinitrophenol; FCCP, carbonyl cyanide 4-trifluoromethoxyphenylhydrazine; TMRE, tetramethylrhodamine, ethyl ester.

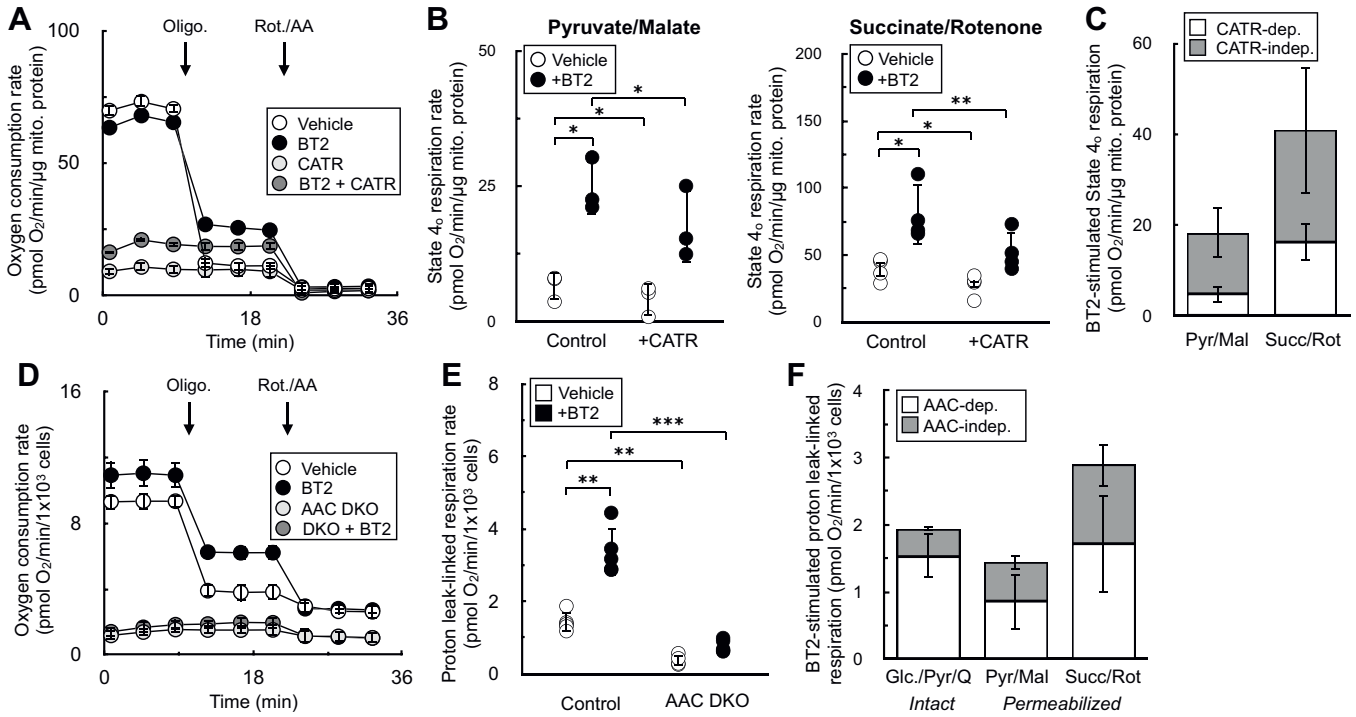

Figure 5. BT2 uncouples *via* both AAC-dependent and AAC-independent mechanisms. *A*, isolated rat liver mitochondria acutely offered 80 µM BT2, 5 µM carboxyatractyloside (CATR), both 80 µM BT2 and 5 µM CATR, or vehicle control 5 min prior to conducting measurements. Mitochondria were offered pyruvate, malate, and ADP as before. (n = 10 technical replicates from a single experiment). *B*, collated state 4_o respiration from experiments as in (*A*) from rat liver mitochondria offered either pyruvate/malate (*left*) or succinate/rotenone (*right*). (n = 4 biological replicates). *C*, collated state 4_o respiration from experiments as in (*A* and *B*) plotted as a stacked bar chart to gauge the proportion of CATR-sensitive (*white*) and CATR-insensitive (*gray*) uncoupling. (n = 4 biological replicates). *D*, intact C2C12 myoblasts with or without genetic ablation of AAC1 and AAC2 (DKO) assayed in DMEM supplemented with glucose, pyruvate, and glutamine as described in the Experimental procedures section. 80 µM BT2 was offered acutely 5 min prior to conducting measurements. (n = 10 technical replicates from a single experiment). *E*, collated proton leak–linked respiration from experiments using intact C2C12 myoblasts as in (*D*). (n = 5 biological replicates). *F*, collated proton leak–linked respiration from experiments as in (*D* and *E*) plotted as a stacked bar chart to gauge the proportion of AAC-dependent (*white*) and AAC-independent (*gray*) uncoupling. Conditions are intact cells offered DMEM supplemented as in (*D*) (*left*) and permeabilized myoblasts offered either pyruvate/malate (*middle*) or succinate/rotenone (*right*). (n = 5 biological replicates). Panels (*B*, *C*, *E*, and *F*) show data as mean ± SD of individual biological replicates. The means are presented for panels (*C* and *F*) rather than individual data points for clarity. Panels (*A* and *D*) show data as mean ± SD from technical replicates. Statistical analysis was conducted with ANOVA followed by Dunnett's posthoc multiple comparison tests. $*p < 0.05$; $**p < 0.01$; $***p < 0.001$. AAC, ADP/ATP carrier; BT2, 3,6-dichlorobenzo[b]thiophene-2-carboxylic acid; DMEM, Dulbecco's modified Eagle's medium.

that AAC inhibition limited the chemical uncoupling independently of the substrate provided (Fig. 5, *B* and *C*). To verify if the results could extend to intact cells, we quantified the effect of BT2 on respiration in C2C12 myoblasts with both *Slc25a4* (encoding AAC1) and *Slc25a5* (encoding AAC2) genetically ablated ("double-knockout") (35). In both intact (Fig. 5, *D*–*F*) and permeabilized cells (Fig. 5*F*), loss of *Aac1* and *Aac2* again resulted in the partial loss of BT2-stimulated uncoupling. In sum, results from both pharmacologic and genetic loss of AAC function point to BT2 having AAC-dependent and AAC-independent mechanisms of mitochondrial uncoupling similar to other well-characterized chemical uncouplers.

BT2 phenocopies DNP and lowers mitochondrial H_2O_2 efflux

Having demonstrated that BT2 can act as a chemical uncoupler distinct from its inhibition of the BCKDK, we next examined whether BT2 can reproduce hallmark biochemical and physiological responses resulting from chemical uncoupling. For example, it is well known that some forms of mitochondrial superoxide production are steeply dependent on the mitochondrial membrane potential (39, 40). As such, even mild chemical uncoupling that fractionally lowers the membrane potential can have a profound effect in lowering mitochondrial ROS production.

Previous work has shown that BT2 treatment reduces ROS production in cells (21). In *in vivo* preclinical heart failure models, BT2 administration preserves cardiac functions known to be sensitive to oxidative stress and protects from ROS-associated I/R and MI injury (12, 20, 21). However, in these systems, it is difficult to discriminate whether the beneficial effects of BT2 result from BCKDK inhibition or other uncharacterized mechanisms. We therefore tested whether BT2 could directly lower mitochondrial superoxide production derived from the respiratory chain.

Isolated rat heart mitochondria were offered succinate to generate superoxide resulting from a high proton motive force and reduced CoQ pool (*i.e.*, "reverse electron transport"). Rates of superoxide production (measured as H_2O_2 efflux) were quantitatively comparable to previous reports (40), and the signal responded appropriately by reporting high rates of superoxide production in the presence of antimycin A (Fig. 6, *A* and *B*) (41). As expected, BT2 significantly reduced

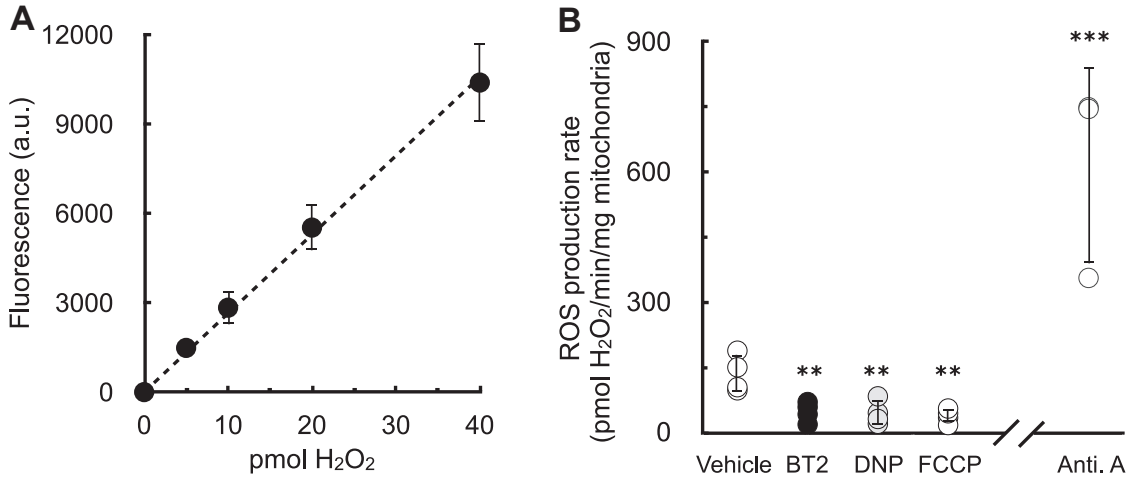

Figure 6. BT2 lowers mitochondrial H_2O_2 efflux. *A*, representative standard curve of exogenous H_2O_2 added on top of isolated mitochondria. (n = 3 technical replicates from a single experiment). *B*, H_2O_2 efflux in isolated mitochondria offered succinate in response to addition of 80 μM BT2, 20 μM DNP, 100 nM FCCP, 1 μM antimycin A, or vehicle control. (n = 3–4 biological replicates). Panel (*A*) shows data as mean ± SD of individual technical replicates. Panel (*B*) shows data as mean ± SD of biological replicates. Statistical analysis was conducted with ANOVA followed by Dunnett's posthoc multiple comparisons tests for the chemical uncouplers. A pairwise Student's *t* test was conducted between vehicle controls and antimycin A. $^{**}p < 0.01$; $^{***}p < 0.001$. BT2, 3,6-dichlorobenzo[b]thiophene-2-carboxylic acid; DNP, 2,4-dinitrophenol; FCCP, carbonyl cyanide 4-trifluoromethoxyphenylhydrazine; H_2O_2, hydrogen peroxide.

mitochondrial H_2O_2 efflux. Importantly, the result could be phenocopied with the chemical uncouplers DNP and FCCP, each of which are structurally dissimilar and have no reported effects on BCKDK. As such, the data indicate that mitochondrial uncoupling could be a mechanism by which BT2 can reduce mitochondrial ROS production independently of BCAA and BCKA metabolism.

BT2 phenocopies DNP and reduces DNL

Although attenuation of mitochondrial ROS production by chemical uncoupling is a plausible mechanism for the cardioprotection afforded by BT2, it almost certainly cannot explain why BT2 protects from insulin resistance and hepatic steatosis. However, another hallmark response to chemical uncouplers is increased energy expenditure. Uncouplers create a "futile cycle" where dissipation of the mitochondrial membrane potential stimulates respiratory chain activity (31, 34). This shifts the energy balance toward nutrient oxidation and away from lipid storage and accumulation. Decades of experimental evidence in rodents and humans support this mechanism (42–45), and chemical uncoupling is consistent with the myriad and sometimes rapid effects of BT2 in various metabolic disease models (26, 46).

We examined whether BT2 could phenocopy DNP in increasing cellular energy expenditure and reducing DNL in differentiated 3T3-L1 adipocytes. Indeed, acute treatment with either BT2 or DNP increased the basal oxygen consumption rate because of increased proton leak–linked respiration (Fig. 7, *A* and *B*). We then conducted stable isotope tracing with uniformly labeled $^{13}C_6$-glucose to further characterize any shared effects of BT2 and DNP. Both compounds increased relative incorporation of glucose into the TCA cycle metabolites citrate and malate (Fig. 7*C*) and decreased the steady-state abundance of these and other TCA cycle intermediates (Fig. 7*D*), a profile consistent with an increased metabolic rate. Taken together, the respirometry and GC–MS data demonstrate that BT2 can increase cellular energy expenditure *via* mitochondrial uncoupling.

Finally, we examined the effect of BT2 and DNP on DNL, reasoning that increased uncoupling would decrease lipid accumulation. Treatment of differentiated 3T3-L1 adipocytes for 72 h with either BT2 or DNP significantly reduced mRNA levels of both a master transcriptional regulator of lipid synthesis (*Srebpf1*) as well as individual enzymes involved in DNL (*Acly*, *Acaca*, and *Fasn*) (Fig. 7*E*). Importantly, levels of *Cpt1a*—the gene encoding carnitine palmitoyltransferase-1a, which is rate controlling for long-chain fatty acid oxidation—were unchanged with DNP and increased with BT2. This result demonstrates that the reduction in DNL genes is not because of toxicity or other experimental artifacts but rather because of a specific shift away from lipid synthesis.

Beyond gene expression, we validated that BT2 reduced DNL by GC–MS analysis of fatty acids. BT2 treatment or DNP treatment for 72 h reduced steady-state levels of myristate (14:0), palmitate (16:0), and stearate (18:0) (Fig. 7*F*). Furthermore, in contrast to increased labeling of TCA cycle intermediates (Fig. 7*C*), incorporation of $^{13}C_6$-glucose into palmitate was decreased in response to administering either compound (Fig. 7*G*). To estimate the rate of palmitate synthesis, we applied isotopomer spectral analysis to model the rate of *de novo* palmitate synthesis [g(t) parameter] and contribution of glucose-derived carbon to the lipogenic acetyl CoA pool ("D" parameter) (47). As in other assays, BT2 and DNP showed qualitative similarities as both decreased the estimated rate of DNL but did not appreciably change the "D" parameter (Fig. 7, *H* and *I* and Table S1). Overall, the gene expression, respiration, and mass spectrometry data show that BT2 phenocopies DNP in increasing energy expenditure and lowering DNL. Thus, the results establish chemical uncoupling

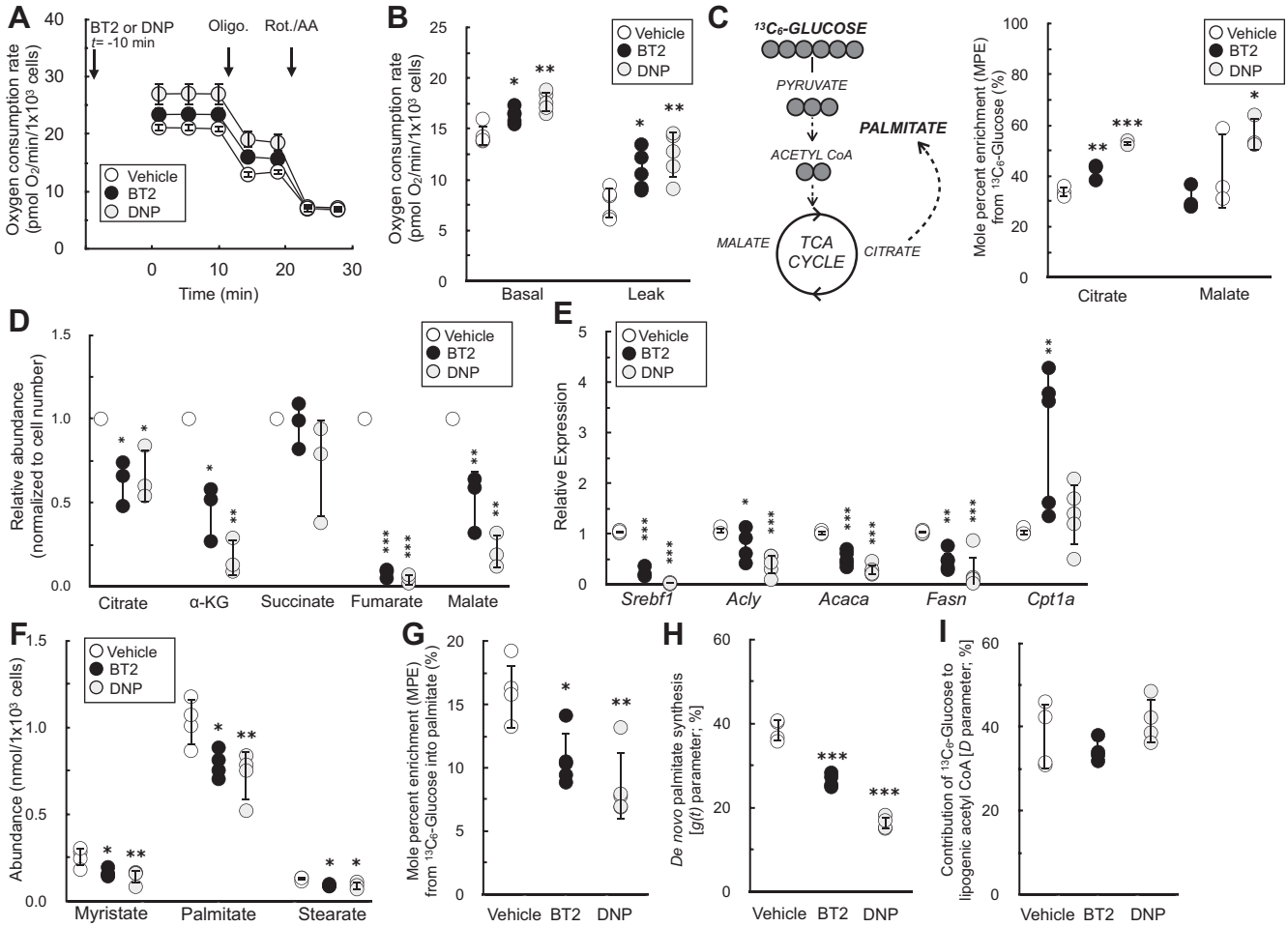

Figure 7. BT2 increases cellular energy expenditure and decreases *de novo* lipogenesis. *A*, representative oxygen consumption trace of differentiated 3T3-L1 adipocytes acutely offered 40 μM BT2 or 10 μM DNP 10 min prior to initial measurements in DMEM supplemented with glucose, pyruvate, and glutamine as described in the Experimental procedures section. (n = 5 technical replicates from a single experiment). *B*, collated oxygen consumption rate parameters for 3T3-L1 cells as in (*A*). (n = 5 biological replicates). *C*, *left*, simplified schematic of uniformly labeled $^{13}C_6$-glucose enriching TCA cycle intermediates and palmitate. *Right*, mole percent enrichment (M.P.E.) from $^{13}C_6$-glucose of TCA cycle intermediates citrate and malate in differentiated 3T3-L1 adipocytes treated for 72 h with 120 μM BT2 or 40 μM DNP in medium containing 2% serum. High concentrations of drug were used to account for drug binding to serum albumin. (n = 3 biological replicates). *D*, relative metabolite abundances of TCA cycle intermediates, adjusted for cell number, for experiments conducted as in (*C*). (n = 3 biological replicates). *E*, quantitative PCR analysis for genes associated with *de novo* lipogenesis as well as *Cpt1a* for cells treated as in (*C*). (n = 5–8 biological replicates). *F*, abundances of fatty acids for experiments conducted as in (*C*). (n = 3–4 biological replicates). *G*, M.P.E. from $^{13}C_6$-glucose into palmitate for experiments conducted as in (*C*). (n = 5 biological replicates). *H*, rate of *de novo* lipogenesis [g(t) parameter] calculated by isotopomer spectral analysis (ISA) for experiments conducted as in (*C*). Averages provided by the model for each biological replicate are presented. Predicted g(t) values and 95% confidence intervals for each technical replicate are provided in Table S1. (n = 4 biological replicates). *I*, fractional contribution of glucose to the lipogenic acetyl CoA pool ("D" parameter) calculated by ISA. Averages provided by the model for each biological replicate are presented. Predicted "D" values and 95% confidence intervals for each technical replicate are provided in Table S1. (n = 4 biological replicates). Panels (*B–I*) show data as mean ± SD of individual biological replicates. Panel (*A*) shows data as mean ± SD from technical replicates. Statistical analysis was conducted with ANOVA followed by Dunnett's posthoc multiple comparison tests. *$p < 0.05$; **$p < 0.01$; and ***$p < 0.001$. BT2, 3,6-dichlorobenzo[b]thiophene-2-carboxylic acid; DMEM, Dulbecco's modified Eagle's medium; DNP, 2,4-dinitrophenol; TCA, tricarboxylic acid.

as a putative mechanism to explain the therapeutic effects of BT2 on cardiometabolic disease (Fig. 8).

Discussion

Here, we provide evidence that the BCKDK inhibitor BT2 is also a chemical uncoupler. Measurements of oxygen consumption, mitochondrial membrane potential, and H^+ conductance all show that BT2 consumes the membrane potential independently of ATP synthesis and uncouples mitochondria. BT2 stimulates proton conductance acutely (<5 min) in reductionist systems bypassing BCKDK activity (*i.e.*, isolated mitochondria offered various substrates as well as patch-clamp electrophysiology of the IMM), demonstrating that it is a *bona fide* chemical uncoupler independent of BCAA metabolism. Chemical uncoupling is a plausible and unifying mechanism for how BT2 can be therapeutic in various models of cardiovascular and metabolic disease independent of its effects on BCAA metabolism.

With respect to heart failure, it is generally accepted that excessive mitochondrial ROS production is an important pathological driver of cardiovascular disease

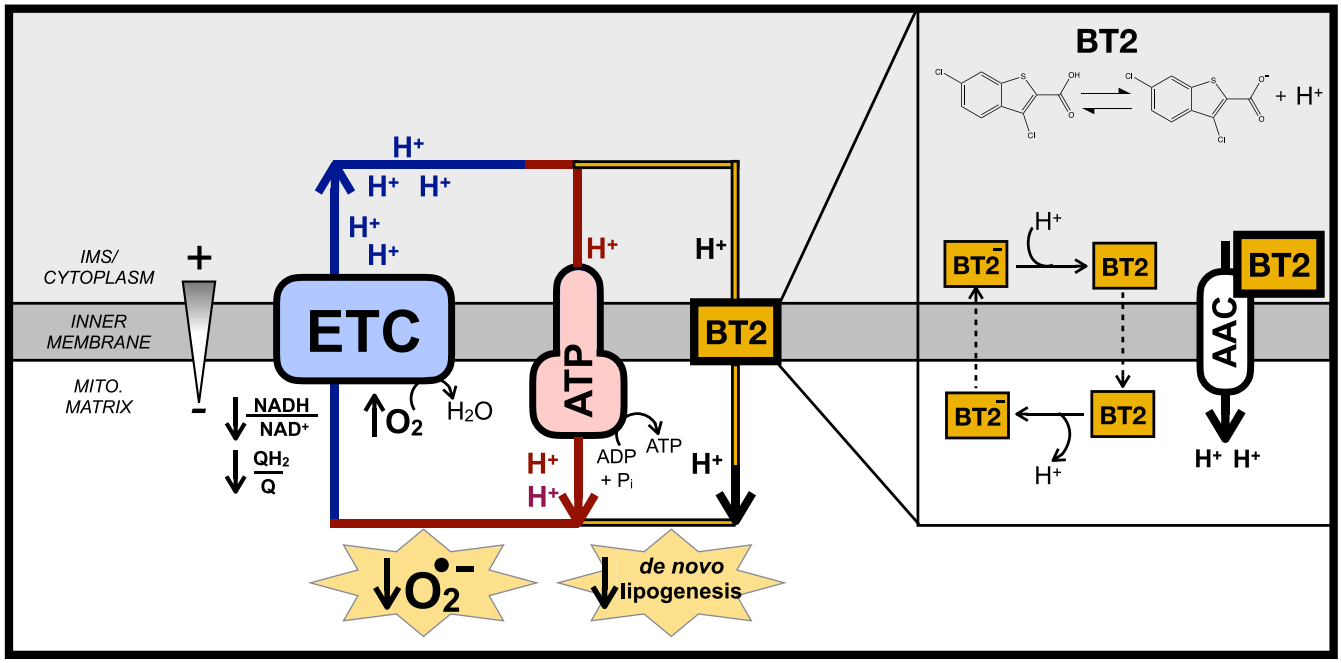

Figure 8. BT2 uncouples mitochondria to increase energy expenditure, lower superoxide production, and reduce *de novo* lipogenesis. AAC, ATP/ADP carrier; ATP, ATP Synthase; BT2, 3,6-dichlorobenzo[b]thiophene-2-carboxylic acid; ETC, electron transport chain; IMS, intermembrane space.

(48–51). A well-known property of uncouplers is limiting mitochondrial superoxide production by lowering the mitochondrial proton motive force, thereby oxidizing the NADH/NAD^+ and QH_2/Q pools and lowering the probability of superoxide formation (39, 52). In addition to a direct effect on reducing mitochondrial ROS production from the respiratory chain, mitochondrial uncoupling is also likely to have an indirect effect in lowering ROS production by blocking induction of the permeability transition pore (53–55). The mitochondrial membrane potential provides the driving force for calcium uptake, and uncoupling mitigates the pathological matrix Ca^{2+} overload that triggers mitochondrial swelling and opening of the permeability transition pore (55, 56). Importantly, both FCCP and DNP confer cardioprotection in *ex vivo* models of I/R injury using the Langendorff-perfused rat heart model (57, 58), and heterologous expression of UCP1 in the mouse heart protects from ischemic damage and lowers markers of oxidative stress (59). These proof-of-concept studies reinforce the notion that attenuation of ROS production *via* chemical uncoupling may explain why BT2 could be cardioprotective independent of its function as a BCKDK inhibitor. Moreover, it should be reinforced that given the steep dependence of ROS production and calcium uptake on the proton motive force, even mild chemical uncoupling that fractionally lowers the membrane potential can have a substantive effect in lowering mitochondrial ROS production (39, 40).

Regarding metabolic disease, it is well known that administration of chemical uncouplers and the resultant increase in energy expenditure can reduce insulin resistance, obesity, and hepatic steatosis in preclinical rodent models (42, 60). In fact, DNP was an effective antiobesity treatment in the 1930s, but a poor safety profile and narrow therapeutic window—rather than a lack of efficacy—discontinued its clinical use (61, 62). Indeed, *in vivo* administration of BT2 in rodents qualitatively mimics the effect of other chemical uncouplers. In various preclinical models, BT2 is protective from glucose intolerance, insulin insensitivity, triglyceride accumulation, and hepatic inflammation similarly to DNP derivatives or Bam15 (22, 24, 26, 29, 46, 63, 64). Several reports demonstrate that BT2 administration does not change body weight (22, 24, 29). However, this may be consistent with a mild uncoupler roughly sixfold less potent than DNP, and BT2 slightly reduces in the respiratory exchange ratio in Zucker fatty rats (22).

The identification of a chemical uncoupling function for BT2 can readily explain some phenomena that are difficult to reconcile with a primary effect on BCAA metabolism. For example, previous reports show that BT2 elicits a rapid euglycemic effect in glucose clamp studies less than an hour after administration (26). Although this time frame is likely inconsistent with remodeling of BCAA metabolism, it is consistent with prior work showing acute effects on energy expenditure by DNP (46). Moreover, our demonstration that DNP phenocopies BT2 in altering gene expression related to lipid metabolism suggests that chemical uncoupling could also explain why BT2 treatment blocks phosphorylation of acetyl CoA carboxylase at multiple sites in a manner not consistent with PP2Cm overexpression (22).

A critical aspect of our finding that BT2 is a chemical uncoupler is determining whether the *in vitro* concentrations required to stimulate uncoupling are relevant for *in vivo* studies. Our observation that BT2 concentrations as low as 2.5 μM increase state 4_o respiration raise the possibility that

BT2 could elicit a mild uncoupling effect given that the concentrations achieved *in vivo* likely approach, if not surpass, the half-maximal inhibitory concentration for BCKDK inhibition (IC_{50} = 3–4 μM) (23). Peak circulating plasma concentrations of BT2 (∼1.0 mM for 40 mg/kg; ∼1.8 mM for 120 mg/kg) (65) and plasma protein binding measurements (99.3% protein bound) (23) suggest that maximal and free BT2 concentrations reach single-digit micromolar concentrations and above. Moreover, pharmacokinetic data indicate a longer half-life in plasma relative to DNP and a clearance profile in plasma more similar to a controlled-release DNP analog (46, 65). Although tissue concentrations are a far more informative parameter, it is likely that BT2 would behave similarly to DNP as a lipophilic membrane-targeting drug that can accumulate in tissues at concentrations at the same order of magnitude as circulating plasma levels (46, 66). Our demonstration that BT2 is roughly a sixfold weaker uncoupler than DNP may help explain why the drug is tolerable at doses that would be egregiously toxic for DNP. In total, available pharmacokinetic data support that chemical uncoupling should be a relevant *in vivo* mechanism for BT2.

BCKDK inhibitors with greater potency than BT2 have been recently developed and evaluated in preclinical models of heart failure and diet-induced obesity (67). For example, the thiophene PF-07208254 has an IC_{50} 10-fold lower than BT2 and protects from transaortic constriction–induced cardiac impairment and high-fat diet–induced metabolic dysfunction. However, despite improved potency, data suggest that PF-07208254 has to be administered at a similar dose to BT2 to elicit comparable *in vivo* results. Indeed, PF-07208254 is also a lipophilic weak acid and comparably sized relative to BT2. Moreover, a series of bulkier thiazole compounds were identified that exhibit extraordinary potency against the BCKDK (∼10^3-fold more potent than BT2) but do not improve metabolic end points (67). These data are consistent with BT2 possessing a mechanism of action discrete from BCKDK activity, and studies examining whether PF-07208254 can act as a chemical uncoupler would be clarifying.

Of course, it may be that other off-target effects of BT2 in addition to chemical uncoupling contribute to observed *in vitro* and *in vivo* phenotypes. For example, recent reports highlight shared pharmacology between angiotensin II type 1 receptor blockers and BT2 (68). Encouragingly, regulation of the renin–angiotensin system may mechanistically explain the effect of BT2 on blood pressure despite *Bckdk* ablation (27), a result unlikely to be directly caused by mitochondrial uncoupling. Additional work suggests that BCKAs can inhibit the mitochondrial pyruvate carrier (69). As BT2 acts as a branched-chain 2-oxoacid analog, it may also inhibit the mitochondrial pyruvate carrier and other mitochondrial transporters or dehydrogenases. In fact, an inhibitory effect on pyruvate metabolism could explain our observation that BT2 stimulates *Cpt1a* expression in differentiated 3T3-L1 adipocytes, whereas DNP does not (70).

In summary, our data suggest that chemical uncoupling by BT2 can explain many of the observed therapeutic benefits attributed to enhanced BCKDH activity and encourage exploration of alternative hypotheses for existing data. For example, overexpression of the PP2Cm can reproduce some of the beneficial effects of BT2, but it is unclear to what extent this is due to BCKDH activity or other targets because of enzyme promiscuity (22, 71). It may also be that the insulin-sensitizing effects of sodium phenylbutyrate (25)—a lipophilic weak acid—are somewhat attributable to chemical uncoupling. Perhaps the strongest evidence against an alternative role for BT2 is the demonstration that the drug does not provide cardioprotection in whole-body *Bckdk*$^{-/-}$ mice (27). However, these animals are characterized by developmental impairments, neurological defects, and growth abnormalities that may warrant cautious interpretation of results (27, 72). Nonetheless, the data demonstrating that BT2 is a chemical uncoupler (i) reinforces the therapeutic promise of chemical uncoupling for a myriad of cardiovascular and metabolic diseases and (ii) further highlights the importance of understanding to what extent BCAA accumulation is causative or associative in cardiovascular and metabolic disease pathogenesis.

Experimental procedures

Animals

All animal protocols and procedures were approved and performed in accordance with the National Institutes of Health Guide for the Care and Use of Laboratory Animals and the UCLA Animal Research Committee. C57BL/6J male mice aged 8 to 12 weeks were purchased from The Jackson Laboratory. Male Sprague–Dawley rats aged between 7 and 10 weeks (∼200–300 g) were purchased from Envigo.

Reagents

BT2 was purchased from MedChemExpress (catalog no.: HY114855), and all other uncouplers were purchased from Sigma–Aldrich (FCCP [catalog no.: C2920], DNP [catalog no.: 42195], and Bam15 [catalog no.: SML-1760]). Stocks were made and stored at −20 °C at the following concentrations: BT2 (40 mM and 400 mM in dimethyl sulfoxide [DMSO]), FCCP (10 mM in 95% ethanol), DNP (20 mM in DMSO), and Bam15 (40 mM in DMSO).

Cell culture

Cardiomyocytes

NRVMs were isolated from postnatal P1–P3-day-old Sprague–Dawley rat pups of mixed sex as previously described (73, 74). Cells were plated onto Agilent Seahorse XF96 cell culture plates or 12-well cell culture dishes coated with 0.1% gelatin (Sigma; catalog no.: G1393) in Dulbecco's modified Eagle's medium (DMEM)/F12 medium (Gibco; catalog no.: 11330057) supplemented with 10% (v/v) fetal bovine serum (FBS), 100 U/ml penicillin, and 100 μg/ml streptomycin. After 24 h, medium was changed to DMEM/F12 lacking FBS but with antibiotics as before. Human iPSC cardiomyocytes (iCell cardiomyocytes; Fujifilm Cellular Dynamics International; catalog no.: 01434) were maintained according to the

manufacturer's guidelines. Cells were grown and maintained in a humidified 5% CO_2 incubator at 37 °C.

3T3-L1 adipocytes

3T3-L1 preadipocytes were purchased directly from the American Type Culture Collection (ATCC) explicitly for use in this study and maintained below 70% confluency in DMEM (Gibco; catalog no.: 11965) supplemented with 10% (v/v) bovine calf serum (ATCC; catalog no.: 30-2020), 100 U/ml penicillin, 100 μg/ml streptomycin, and 1 mM sodium pyruvate. Cells were plated onto XF96 cell culture plates or 12-well tissue culture dishes and allowed to grow for 48 h (plating on day −2). On day 0, differentiation was begun by changing the medium to maintenance medium (DMEM supplemented with 10% [v/v] FBS, 100 U/ml penicillin, 100 μg/ml streptomycin, 1 mM sodium pyruvate, 10 mM Hepes) further supplemented with 1 μg/ml insulin (Sigma; catalog no.: I0515), 0.25 μM dexamethasone (Sigma; catalog no.: D4904), 0.5 mM methylisobutylxanthine (Sigma; catalog no.: I5879), and 100 nM rosiglitazone (Sigma; catalog no.: R2408). On day 2, medium was changed to maintenance medium supplemented only with 1 μg/ml insulin, and on days 4 and 6, medium was replaced to maintenance medium with no further additions. Cells were treated with compound on day 8 as described elsewhere in the Experimental procedures section. Cell lines were free from mycoplasma contamination for all experiments.

C2C12 myoblasts

C2C12 myoblasts were purchased directly from ATCC explicitly for use in this study and maintained in DMEM (Gibco; catalog no.: 11965) supplemented with 10% (v/v) FBS, 100 U/ml penicillin, 100 μg/ml streptomycin, and 1 mM sodium pyruvate. Cells with genetic ablation of *Slc25a4* and *Slc25a5* (encoding AAC1 and AAC2) were generated and described previously (35). Cell lines were free from mycoplasma contamination for all experiments.

HepG2 hepatocytes

HepG2 hepatocytes purchased directly from ATCC explicitly for use in this study and were maintained in MEM (Gibco; catalog no.: 11095) supplemented with 10% (v/v) FBS, 100 U/ml penicillin, 100 μg/ml streptomycin, and 2 mM GlutaMAX. Cell lines were free from mycoplasma contamination for all experiments.

Mitochondrial isolation

Mitochondrial isolation from rodent heart and liver was conducted according to well-established protocols (75) and all steps were conducted on ice or at 4 °C. Mitochondrial protein content was measured by the bicinchoninic acid assay.

Liver mitochondria

Mouse livers or rat livers were cleaned, minced, and drained of blood in ice-cold MSHE (210 mannitol, 70 mM sucrose, 5 mM Hepes, 1 mM EGTA, and 0.2% [w/v] fatty acid–free serum albumin [BSA]) at pH 7.2 at 4 °C. Livers were disrupted using two strokes of a drill-driven Teflon-on-glass Dounce homogenizer with roughly 1 ml of buffer for every 100 mg of tissue. The homogenate was spun at 12,000*g* for 10 min at 4 °C to remove any contaminating fat. The pellet was resuspended and centrifuged at 800*g* for 5 min at 4 °C to remove debris. The supernatant was filtered through two layers of wet cheesecloth and centrifuged at 12,000*g* for 10 min at 4 °C. The light, "fluffy" layer of the pellet was removed, and the mitochondrial pellet was resuspended and centrifuged again at 12,000*g* at 4 °C. For the third and final centrifugation step, the pellet was washed and resuspended in MSHE lacking BSA and centrifuged again at 4 °C. The final mitochondrial pellet was resuspended in MSHE lacking BSA and kept at a concentration greater than 100 mg/ml and kept on ice.

Heart mitochondria

Mouse hearts or rat hearts were quickly removed from the euthanized animal while still beating and minced, cleaned off blood, and homogenized using a hand-held tissue disruptor (IKA Ultra-Turrax) in ice-cold MSHE. The homogenate was centrifuged at 900*g* for 10 min at 4 °C. The supernatant was then centrifuged at 9000*g* for 10 min at 4 °C, and the remaining pellet was washed and recentrifuged at 9000*g* at 4 °C in medium lacking BSA. The final mitochondrial pellet was resuspended in MSHE lacking BSA and kept at a concentration greater than 25 mg/ml and kept on ice.

Respirometry

All oxygen consumption measurements were conducted using an Agilent Seahorse XF96 or XF^{e}96 Analyzer. Experiments were conducted at 37 °C and at pH 7.4 (intact cells) or 7.2 (isolated mitochondria and permeabilized cells). For experiments with intact cells or permeabilized cells, only the inner 60 wells were used and the outer rim was filled with 200 μl of PBS throughout the incubation to minimize variance in temperature and evaporative effects across the plate. All respiratory parameters were corrected for nonmitochondrial respiration and background signal from the instrument with addition of 200 nM rotenone and 1 μM antimycin A and calculated according to well-established best practices (30, 76).

Intact cells

Respiration was measured in NRVMs (4.0×10^4 cells/well), iPSC cardiomyocytes (1.5×10^4 cells/well), C2C12 myoblasts (1.5×10^4 cells/well), and differentiated 3T3-L1 adipocytes (2.5×10^3 cells/well) in DMEM assay medium composed of DMEM (Sigma; catalog no.: 5030) supplemented with 31.6 mM NaCl, 3 mg/l phenol red, 5 mM Hepes, 10 mM glucose, 2 mM glutamine, and 2 mM pyruvate. Where appropriate, cells were offered oligomycin (2 μM), and maximal respiration was estimated with 750 nM FCCP.

Permeabilized cells

Cells were permeabilized with 3 nM recombinant perfringolysin O and assayed as previously described (77) in MAS

buffer (220 mM mannitol, 70 mM sucrose, 10 mM KH_2PO_4, 5 mM $MgCl_2$, 2 mM Hepes [pH 7.2 at 37 °C], 1 mM EGTA, 0.2% [w/v] BSA). Where indicated medium was supplemented with 4 mM ADP and 10 mM pyruvate with 1 mM malate, 5 mM glutamate with 5 mM malate, or 10 mM succinate with 2 μM rotenone. Oligomycin (2 μM) and rotenone (200 nM) with antimycin A (1 μM) were offered during the course of the assay to calculate respiratory parameters according to standard practice.

Isolated mitochondria

Oxygen consumption rates in isolated mitochondria were measured in MAS buffer described previously according to well-established protocols (77, 78). As indicated in the figure legends, BSA was either omitted from the assay medium or used at 0.001% (w/v) to avoid sequestering lipophilic compounds under investigation. Where indicated, MAS buffer was supplemented with 10 mM pyruvate with 1 mM malate (Pyr/Mal), 5 mM glutamate with 5 mM malate (Glu/Mal), or 10 mM succinate with 2 μM rotenone (Succ/Rot). Mitochondria were offered oligomycin at 2 μM and FCCP at 1 μM where indicated.

Normalization

All intact and permeabilized cell oxygen consumption rates were normalized to cell number. Cells were immediately fixed after the assay with 2% (v/v) paraformaldehyde in PBS and stored at 4 °C for up to 14 days. Nuclei were stained with Hoechst (ThermoFisher; catalog no.: 33342) overnight at 4 °C and quantified using the Operetta High Content Imaging System (PerkinElmer). All oxygen consumption rates in isolated mitochondria were normalized to microgram of total mitochondrial protein in the microplate well unless otherwise indicated.

Mitochondrial membrane potential

Isolated mitochondria

The mitochondrial membrane potential was measured using the quenched fluorescence using a high concentration of TMRE as has been previously described (79). TMRE fluorescence will self-quench upon accumulation in the mitochondrial matrix at high concentrations. As such, lowering the membrane potential will decrease dye uptake and self-quenching, thereby increasing the observed fluorescent signal. Mitochondria isolated from rat liver or rat heart (0.6 mg/ml) were incubated in MAS buffer supplemented with 0.001% BSA, 4 mM ADP, 5 mM succinate, 2 μM rotenone, and 5 μM TMRE at 37 °C for 10 min in a black-walled 96-well microplate shielded from light. After incubation, fluorescence was measured (549 excitation/575 emission) using a Tecan Spark multimode plate reader. Compounds under investigation were immediately added prior to the 10 min incubation period.

Cardiomyocytes

The mitochondrial membrane potential in cells was measured with TMRE using the Image Xpress Micro Confocal High-Content Imaging System (Molecular Devices). NRVMs and iPSC-derived iCell cardiomyocytes were plated onto collagen-coated and black-walled PhenoPlates (PerkinElmer) at either 6.0×10^4 (NRVMs) or 1.5×10^4 (iCell) cells/well and maintained as described earlier in the Experimental procedures section. About 75 min prior to conducting measurements, medium was exchanged for DMEM lacking glucose, phenol red, and sodium bicarbonate (Sigma; catalog no.: 5030) supplemented with 31.6 mM NaCl, 10 mM glucose, 2 mM glutamine, 2 mM pyruvate, and 5 mM Hepes along with 10 nM TMRE (Invitrogen; catalog no.: T669) and 200 nM MitoTracker Green FM (MTG; catalog no.: M7514). After allowing the dyes to equilibrate for 1 h, BT2 (80 μM), DNP (10 μM), and FCCP (1 μM) were added. Plates were treated with compounds of interest and immediately transported to the core facility where the plate was put into the instrument. Measurements are listed 20 to 40 min after treatment to reflect the time from which the cells were treated with drug until the measurements were taken in the last microplate wells. The plating schemes for each of the biological replicates were altered (*i.e.*, at times the control group was in the left corner of the plate that was initially read by the instrument; during other experiments, the drug treatments were in this position) so that temporal differences in how the plate was read could not skew any results.

Images were acquired with the 50 μm slit confocal mode and a 40× (1.2 numerical aperture) water lens in Z-stack mode of 1 μm slices with a total of six slices. Analysis was performed in the MetaXpress (Molecular Devices) software clamping the analysis parameters for all acquired images. Maximum Z-projections of MTG were used for morphologic analysis, and the sum of Z-projections of TMRE was used for quantification of intensity. A TopHat filter was applied on the MTG images for better definition of structures and equalization of fluorescence. The images were thresholded and transformed into a binary segmentation. This segmented area was used to measure the average intensity of TMRE and the circularity of mitochondria. Circularity is defined with "1" being a perfect circle and "0" a straight line.

Patch-clamp recordings

Proton conductance across the IMM was conducted on mitoplasts derived from mouse heart mitochondria as previously described (35, 80). Mitoplasts isolated from heart mitochondria have been used previously to characterize other H^+ currents induced by compounds such as free fatty acids and chemical uncouplers including DNP and FCCP. Cardiac mitoplasts are well accepted as representative of the non-adipose tissue H^+ current and exhibit similar biophysical characteristics with skeletal muscle and liver. Patch-clamp recording was performed from isolated heart mitoplasts of mice. The mitoplasts used for patch-clamp experiments were 3 to 5 μm in diameter and typically had membrane capacitances of 0.3 to 1.2 pF. Both the bath and pipette solutions were formulated to record H^+ currents and contained only salts that dissociate into large anions and cations that are normally impermeant through ion channels or transporters. A low pH

gradient across the IMM was used (pH 7.5 and 7.0 on the matrix and cytosolic sides, respectively).

Pipettes were filled with 130 mM tetramethylammonium hydroxide, 1 mM EGTA, 2 mM Tris–HCl, and 100 mM Hepes. pH was adjusted to 7.5 with D-gluconic acid, and tonicity was adjusted to ∼360 mmol/kg with sucrose. Typically, pipettes had resistances of 25 to 35 MΩ, and the access resistance was 40 to 75 MΩ. Whole-mitoplast I_H was recorded in the bath solution containing 100 mM Hepes and 1 mM EGTA (pH adjusted to 7 with Trizma base, and tonicity adjusted to ∼300 mmol/kg with sucrose). All experiments were performed under continuous perfusion of the bath solution. All electrophysiological data presented were acquired at 10 kHz and filtered at 1 kHz.

H_2O_2 efflux

H_2O_2 efflux was measured in isolated mitochondria as described previously (40) using a Tecan Spark multimode plate reader and an Amplex Red–based detection system. Mitochondria (2 mg/ml) were incubated in SHE buffer (250 mM sucrose, 10 mM Hepes, 1 mM EGTA, pH 7.2 at 37 °C) supplemented with 2.5 μM Amplex Red (ThermoFisher; catalog no.: A12222) and 5 U/ml horseradish peroxidase (ThermoFisher; catalog no.: 31491). About 10 mM succinate was added to the incubation, and the rate of H_2O_2 was measured over 2 to 3 min. The signal was calibrated to known amounts of H_2O_2 added on top of isolated mitochondria. Compounds under investigation were preincubated with mitochondria in SHE buffer for 2 to 5 min prior to the addition of succinate.

Stable isotope tracing and DNL

Cell culture

3T3-L1 adipocytes—3T3-L1 preadipocytes were seeded at 2.5×10^4 cells/well in 12-well dishes and differentiated as described earlier in the Experimental procedures section. On day 8, cells were changed into maintenance medium (made with DMEM; catalog no.: A1443001) with the following changes: 2% (v/v) FBS rather than 10% to reduce protein binding of compounds under investigation, and uniformly labeled [$^{13}C_6$]-glucose (Cambridge Isotope Laboratories; catalog no.: CLM-1396) was used instead of ^{12}C-unlabeled glucose. BT2 (120 μM) and DNP (40 μM) were added during this step and used at higher concentrations than in other experiments to account for binding to albumin in 2% (v/v) FBS. After 72 h, cells were extracted for GC–MS analysis as described later. A matched 12-well dish was used for normalization of metabolite levels to cell number. On the day of the extraction, cells were fixed with 2% (v/v) paraformaldehyde in PBS and stored at 4 °C for no less than 7 days. Nuclei were stained with Hoescht (ThermoFisher; catalog no.: 33342) overnight at 4 °C and quantified using the Operetta High Content Imaging System (PerkinElmer).

NRVMs—NRVMs were seeded at 4.0×10^5 cells/well in 12-well dishes coated with 0.1% (w/v) gelatin in DMEM/F12 medium described earlier. After 24 h, medium was exchanged into custom DMEM formulated without glucose, glutamine, or leucine (Sciencell Laboratories) and supplemented with 10 mM glucose, 2 mM GlutaMAX, or 0.8 mM leucine, with a uniformly labeled [$^{13}C_6$] label on either glucose or leucine (catalog no.: CLM-2262). After 24 h, cells were extracted for GC–MS analysis as described later.

Immortalized cell lines—C2C12 myoblasts (2.0×10^5 cells/well) or HepG2 hepatocytes (4.0×10^5 cells/well) were seeded into 6-well dishes. After 24 h, medium was exchanged into custom DMEM formulated without glucose, glutamine, or leucine (Sciencell Laboratories) and supplemented with 10 mM glucose, 2 mM glutamine, or 0.8 mM leucine, with a uniform ^{13}C label on either glucose, leucine, or glutamine (catalog no.: CLM-1822). After 24 h, cells were extracted for GC–MS analysis as described later.

Derivatization and mass spectrometry

Cell preparation and stable isotope tracing measuring incorporation of isotopic labels into polar metabolites and palmitate was conducted as previously described (81, 82). Metabolite extraction was conducted with a Folch-like method using a 5:2:5 ratio of methanol:water:chloroform. About 12-well dishes were kept on ice and quickly washed with ice-cold 0.9% (w/v) NaCl. Cells were then scraped in ice-cold methanol and water containing 5 μg/ml norvaline (Sigma; catalog no.: N7502), an internal standard. Chloroform containing 20 μM [U-$^2H_{31}$]-palmitate (Cambridge Isotope Laboratories; catalog no.: DLM-215) as an internal standard was then added to the samples. Samples were then vortexed for 1 min and centrifuged at 10,000*g* for 5 min at 4 °C.

The polar fraction (top layer) was removed, and the samples were dried overnight using a refrigerated CentriVap vacuum concentrator (LabConco). Metabolites (50 nmol to 23 pmol) were extracted alongside the cell samples to ensure the signal fell within the linear detection range of the instrument. The dried polar metabolites were reconstituted in 20 μl of 2% (w/v) methoxyamine in pyridine prior to a 45 min incubation at 37 °C. Subsequently, 20 μl of MTBSTFA with 1% tert-butyldimethylchlorosilane was added to samples, followed by an additional 45 min incubation at 37 °C. Samples were analyzed using Agilent MassHunter software, and FluxFix software (http://fluxfix.science) was used to correct for the abundance of natural heavy isotopes against an in-house reference set of unlabeled metabolite standards (83).

The lower organic fraction was dried under air and then solubilized in 500 μl of acidified methanol (2% [v/v] H_2SO_4 in methanol) for 2 h at 50 °C to generate fatty acid methyl esters (FAMEs). After this incubation, 100 μl of saturated NaCl was added, followed by 500 μl of hexane. This mixture was vortexed for 2 min, and the upper hexane layer was collected in a new microfuge tube. An additional 500 μl of hexane was added to the original MeOH–NaCl tube, and the process was repeated to collect any residual FAMEs not obtained by the first addition. The pooled hexane extracts were then dried under airflow and resuspended in 75 μl of hexane. FAMEs were analyzed by GC–MS analysis. *De novo* lipid synthesis was estimated by isotopomer spectral analysis (47, 82) and calculated using MATLAB (MathWorks) software.

Samples were analyzed using a DB-35 column (Agilent Technologies). Information regarding additional technical specifications is available elsewhere (81, 82).

Quantitative PCR

3T3-L1 adipocytes were plated, maintained, and treated with either BT2 or DNP in 12-well dishes identically to those used for GC–MS analysis. Transcript levels were measured using quantitative PCR. RNA was extracted using the RNeasy Mini Kit (Qiagen; catalog no.: 74106), and complementary DNA was generated using the High-Capacity cDNA Reverse Transcription Kit (Applied Biosystems; catalog no.: 4368814). The PowerUp SYBR Green Master Mix kit (Applied Biosystems; catalog no.: A25743) and a QuantStudio 5 (Applied Biosystems) were used for quantitative PCR analysis. Relative gene expression was calculated using the $\Delta\Delta C_t$ method with *36b4* as a reference gene.

Statistical analysis

All statistical parameters, including the number of biological replicates (n), can be found in the figure legends. Statistical analyses were performed using GraphPad Prism 5 software (GraphPad Software, Inc). Data are presented as the mean ± standard deviation unless otherwise specified. Where appropriate, individual data points representing values from each independent biological replicate are presented, in accordance with the American Society for Biochemistry and Molecular Biology best practices. Individual pairwise comparisons were performed using two-tailed Student's *t* test. For analysis involving more than two groups, data were analyzed by repeated-measures ANOVA followed by Dunnett's post hoc multiple comparison tests (compared against vehicle controls unless otherwise specified). Data were assumed to follow a normal distribution (no tests were performed). Values denoted as follows were considered statistically significant: $^{*}p < 0.05$; $^{**}p < 0.01$; and $^{***}p < 0.001$.

Data availability

All data supporting the findings in this study are available from the corresponding author upon request.

Supporting information—This article contains supporting information.

Author contributions—A. A., A. S. D., and Y. W. conceptualization; A. A., A. E. J., B. D., C. B., L. S., M. W., A. M. B., and A. S. D. methodology; A. A., A. E. J., B. D., R. T., C. B., M. W., A. M. B., and A. S. D. formal analysis; A. A., A. E. J., B. D., K. P. M., C. B., L. S., A. M. B., and A. S. D. investigation; O. S. S., M. W., Y. W., A. M. B., and A. S. D. resources; A. A., A. E. J., R. T., C. B., M. W., A. M. B., and A. S. D. data curation; A. A. and A. S. D. writing–original draft; A. A., A. E. J., B. D., R. T., K. P. M., C. B., K. R., O. S. S., L. S., M. W., Y. W., A. M. B., and A. S. D. writing–review & editing; A. A., K. R., O. S. S., Y. W., A. M. B., and A. S. D. supervision; K. R., O. S. S., Y. W., and A. S. D. project administration; M. W., Y. W., A. M. B., and A. S. D. funding acquisition.

Funding and additional information—A. S. D. is supported by the National Institutes of Health grants R35GM138003 and P30DK063491 as well as the W. M. Keck Foundation (grant no.: 995337) and the Agilent Early Career Professor Award. A. M. B. is supported by the National Institutes of Health grant R35GM143097 and the Pew Scholars in Biomedical Sciences. Y. W. is supported by the Department of Defense CDMRP (grant no.: PR191670). R. T. and M. W. are supported by an Ad Astra Fellowship. A. E. J. was supported by the UCLA Tumor Cell Biology Training Program (grant no.: T32 CA009056). The content is solely the responsibility of the authors and does not necessarily represent the official views of the National Institutes of Health.

Conflict of interest—Y. W. is a scientific founder and paid consultant for Ramino Therapeutics. A. S. D. has previously served as a paid consultant for Agilent Technologies.

Abbreviations—The abbreviations used are: AAC, ADP/ATP carrier; ATCC, American Type Culture Collection; BCAA, branched chain amino acid; BCKA, branched-chain α-ketoacid; BCKDH, branched-chain α-ketoacid dehydrogenase; BSA, bovine serum albumin; BT2, 3,6-dichlorobenzo[b]thiophene-2-carboxylic acid; DMEM, Dulbecco's modified Eagle's medium; DMSO, dimethyl sulfoxide; DNL, *de novo* lipogenesis; DNP, 2,4-dinitrophenol; FAME, fatty acid methyl ester; FBS, fetal bovine serum; FCCP, carbonyl cyanide 4-trifluoromethoxyphenylhydrazine; H2O2, hydrogen peroxide; IMM, inner mitochondrial membrane; iPSC, induced pluripotent stem cell; I/R, ischemia/reperfusion; MI, myocardial infarction; MTG, MitoTracker Green FM; NRVM, neonatal rat ventricular myocyte; PP2Cm, protein phosphatase 2Cm; ROS, reactive oxygen species; TCA, tricarboxylic acid; TMRE, tetramethylrhodamine, ethyl ester.

References

1. McGarrah, R. W., and White, P. J. (2023) Branched-chain amino acids in cardiovascular disease. *Nat. Rev. Cardiol.* **20**, 77–89
2. White, P. J., and Newgard, C. B. (2019) Branched-chain amino acids in disease. *Science (New York, N.Y.)* **363**, 582–583
3. Sun, H., and Wang, Y. (2016) Branched chain amino acid metabolic reprogramming in heart failure. *Biochim. Biophys. Acta Mol. Basis Dis.* **1862**, 2270–2275
4. Neinast, M., Murashige, D., and Arany, Z. (2019) Branched chain amino acids. *Annu. Rev. Physiol.* **81**, 139–164
5. Vanweert, F., Schrauwen, P., and Phielix, E. (2022) Role of branched-chain amino acid metabolism in the pathogenesis of obesity and type 2 diabetes-related metabolic disturbances BCAA metabolism in type 2 diabetes. *Nutr. Diabetes* **12**, 35
6. Felig, P., Marliss, E., and Cahill, G. F. (1969) Plasma amino acid levels and insulin secretion in obesity. *New Engl. J. Med.* **281**, 811–816
7. White, P. J., McGarrah, R. W., Herman, M. A., Bain, J. R., Shah, S. H., and Newgard, C. B. (2021) Insulin action, type 2 diabetes, and branched-chain amino acids: a two-way street. *Mol. Metab.* **52**. https://doi.org/10.1016/J.MOLMET.2021.101261
8. Newgard, C. B., An, J., Bain, J. R., Muehlbauer, M. J., Stevens, R. D., Lien, L. F., *et al.* (2009) A branched-chain amino acid-related metabolic signature that differentiates obese and lean humans and contributes to insulin resistance. *Cell Metab.* **9**, 311–326
9. Wang, T. J., Larson, M. G., Vasan, R. S., Cheng, S., Rhee, E. P., McCabe, E., *et al.* (2011) Metabolite profiles and the risk of developing diabetes. *Nat. Med.* **17**, 448–453
10. Flores-Guerrero, J. L., Groothof, D., Connelly, M. A., Otvos, J. D., Bakker, S. J. L., and Dullaart, R. P. F. (2019) Concentration of branched-chain amino acids is a strong risk marker for incident hypertension. *Hypertension* **74**, 1428–1435

11. Tobias, D. K., Lawler, P. R., Harada, P. H., Demler, O. V., Ridker, P. M., Manson, J. A. E., *et al.* (2018) Circulating branched-chain amino acids and incident cardiovascular disease in a prospective cohort of US women. *Circ. Genomic Precision Med.* **11**, e002157
12. Sun, H., Olson, K. C., Gao, C., Prosdocimo, D. A., Zhou, M., Wang, Z., *et al.* (2016) Catabolic defect of branched-chain amino acids promotes heart failure. *Circulation* **133**, 2038–2049
13. Bhattacharya, S., Granger, C. B., Craig, D., Haynes, C., Bain, J., Stevens, R. D., *et al.* (2014) Validation of the association between a branched chain amino acid metabolite profile and extremes of coronary artery disease in patients referred for cardiac catheterization. *Atherosclerosis* **232**, 191–196
14. Portero, V., Nicol, T., Podliesna, S., Marchal, G. A., Baartscheer, A., Casini, S., *et al.* (2022) Chronically elevated branched chain amino acid levels are pro-arrhythmic. *Cardiovasc. Res.* **118**, 1742
15. Shah, S. H., Sun, J. L., Stevens, R. D., Bain, J. R., Muehlbauer, M. J., Pieper, K. S., *et al.* (2012) Baseline metabolomic profiles predict cardiovascular events in patients at risk for coronary artery disease. *Am. Heart J.* **163**, 844–850.e1
16. Lu, G., Sun, H., She, P., Youn, J. Y., Warburton, S., Ping, P., *et al.* (2009) Protein phosphatase 2Cm is a critical regulator of branched-chain amino acid catabolism in mice and cultured cells. *J. Clin. Invest.* **119**, 1678–1687
17. Harris, R. A., Joshi, M., Jeoung, N. H., and Obayashi, M. (2005) Overview of the molecular and biochemical basis of branched-chain amino acid catabolism. *J. Nutr.* **135**. https://doi.org/10.1093/JN/135.6.1527S
18. Cummings, N. E., Williams, E. M., Kasza, I., Konon, E. N., Schaid, M. D., Schmidt, B. A., *et al.* (2018) Restoration of metabolic health by decreased consumption of branched-chain amino acids. *J. Physiol.* **596**, 623–645
19. Wang, W., Zhang, F., Xia, Y., Zhao, S., Yan, W., Wang, H., *et al.* (2016) Defective branched chain amino acid catabolism contributes to cardiac dysfunction and remodeling following myocardial infarction. *Am. J. Physiol. Heart Circ. Physiol.* **311**, H1160–H1169
20. Li, T., Zhang, Z., Kolwicz, S. C., Raftery, D., Sun, H., and Correspondence, R. T. (2017) Defective branched-chain amino acid catabolism disrupts glucose metabolism and sensitizes the heart to ischemia-reperfusion injury. *Cell Metab.* **25**, 374–385
21. Lian, K., Guo, X., Wang, Q., Liu, Y., Wang, R. T., Gao, C., *et al.* (2020) PP2Cm overexpression alleviates MI/R injury mediated by a BCAA catabolism defect and oxidative stress in diabetic mice. *Eur. J. Pharmacol.* **866**. https://doi.org/10.1016/J.EJPHAR.2019.172796
22. White, P. J., McGarrah, R. W., Grimsrud, P. A., Tso, S. C., Yang, W. H., Haldeman, J. M., *et al.* (2018) The BCKDH kinase and phosphatase integrate BCAA and lipid metabolism via regulation of ATP-citrate lyase. *Cell Metab.* **27**, 1281–1293.e7
23. Tso, S. C., Gui, W. J., Wu, C. Y., Chuang, J. L., Qi, X., Skvorak, K. J., *et al.* (2014) Benzothiophene carboxylate derivatives as novel allosteric inhibitors of branched-chain α-ketoacid dehydrogenase kinase. *J. Biol. Chem.* **289**, 20583
24. Zhou, M., Shao, J., Wu, C. Y., Shu, L., Dong, W., Liu, Y., *et al.* (2019) Targeting BCAA catabolism to treat obesity-associated insulin resistance. *Diabetes* **68**, 1730–1746
25. Vanweert, F., Neinast, M., Tapia, E. E., van de Weijer, T., Hoeks, J., Schrauwen-Hinderling, V. B., *et al.* (2022) A randomized placebo-controlled clinical trial for pharmacological activation of BCAA catabolism in patients with type 2 diabetes. *Nat. Commun.* **13**. https://doi.org/10.1038/S41467-022-31249-9
26. Bollinger, E., Peloquin, M., Libera, J., Albuquerque, B., Pashos, E., Shipstone, A., *et al.* (2022) BDK inhibition acts as a catabolic switch to mimic fasting and improve metabolism in mice. *Mol. Metab.* **66**. https://doi.org/10.1016/J.MOLMET.2022.101611
27. Murashige, D., Jung, J. W., Neinast, M. D., Levin, M. G., Chu, Q., Lambert, J. P., *et al.* (2022) Extra-cardiac BCAA catabolism lowers blood pressure and protects from heart failure. *Cell Metab.* **34**, 1749–1764.e7
28. Murashige, D., Jang, C., Neinast, M., Edwards, J. J., Cowan, A., Hyman, M. C., *et al.* (2020) Comprehensive quantification of fuel use by the failing and nonfailing human heart. *Science (New York, N.Y.)* **370**, 364–368
29. Blair, M. C., Neinast, M. D., Jang, C., Chu, Q., Jung, J. W., Axsom, J., *et al.* (2023) Branched-chain amino acid catabolism in muscle affects systemic BCAA levels but not insulin resistance. *Nat. Metab.* **5**, 589–606
30. Divakaruni, A. S., and Jastroch, M. (2022) A practical guide for the analysis, standardization and interpretation of oxygen consumption measurements. *Nat. Metab.* **4**, 978–994
31. Divakaruni, A. S., and Brand, M. D. (2011) The regulation and physiology of mitochondrial proton leak. *Physiology (Bethesda, Md.)*. https://doi.org/10.1152/physiol.00046.2010
32. Brand, M. D., and Nicholls, D. G. (2011) Assessing mitochondrial dysfunction in cells. *Biochem. J.* https://doi.org/10.1042/BJ20110162
33. Orr, A. L., Quinlan, C. L., Perevoshchikova, I. V., and Brand, M. D. (2012) A refined analysis of superoxide production by mitochondrial sn-glycerol 3-phosphate dehydrogenase. *J. Biol. Chem.* **287**, 42921–42935
34. Bertholet, A. M., and Kirichok, Y. (2022) Mitochondrial H + leak and thermogenesis. *Annu. Rev. Physiol.* **84**, 381–407
35. Bertholet, A. M., Natale, A. M., Bisignano, P., Suzuki, J., Fedorenko, A., Hamilton, J., *et al.* (2022) Mitochondrial uncouplers induce proton leak by activating AAC and UCP1. *Nature* **606**, 180–187
36. Nicholls, D. G., and Ferguson, S. J. (2013) *Bioenergetics*, 4th, Academic Press, London
37. Andreyev, A. Y., Bondareva, T. O., Dedukhova, V. I., Mokhova, E. N., Skulachev, V. P., and Volkov, N. I. (1988) Carboxyatractylate inhibits the uncoupling effect of free fatty acids. *FEBS Lett.* **226**, 265–269
38. Lou, P. H., Hansen, B. S., Olsen, P. H., Tullin, S., Murphy, M. P., and Brand, M. D. (2007) Mitochondrial uncouplers with an extraordinary dynamic range. *Biochem. J.* **407**, 129–140
39. Korshunov, S. S., Skulachev, V. P., and Starkov, A. A. (1997) High protonic potential actuates a mechanism of production of reactive oxygen species in mitochondria. *FEBS Lett.* **416**, 15–18
40. Robb, E. L., Hall, A. R., Prime, T. A., Eaton, S., Szibor, M., Viscomi, C., *et al.* (2018) Control of mitochondrial superoxide production by reverse electron transport at complex I. *J. Biol. Chem.* https://doi.org/10.1074/jbc.RA118.003647
41. Affourtit, C., Quinlan, C. L., and Brand, M. D. (2012) Measurement of proton leak and electron leak in isolated mitochondria. *Methods Mol. Biol.* https://doi.org/10.1007/978-1-61779-382-0_11
42. Goedeke, L., Perry, R. J., and Shulman, G. I. (2019) Emerging pharmacological targets for the treatment of nonalcoholic fatty liver disease, insulin resistance, and type 2 diabetes. *Annu. Rev. Pharmacol. Toxicol.* **59**, 65–87
43. Childress, E. S., Alexopoulos, S. J., Hoehn, K. L., and Santos, W. L. (2018) Small molecule mitochondrial uncouplers and their therapeutic potential. *J. Med. Chem.* **61**, 4641–4655
44. Kajimura, S., and Saito, M. (2014) A new era in Brown adipose tissue Biology: molecular control of Brown fat development and energy homeostasis. *Annu. Rev. Physiol.* **76**, 225–249
45. Cannon, B., and Nedergaard, J. (2004) Brown adipose tissue: function and physiological significance. *Physiol. Rev.* https://doi.org/10.1152/physrev.00015.2003
46. Perry, R. J., Zhang, D., Zhang, X. M., Boyer, J. L., and Shulman, G. I. (2015) Controlled-release mitochondrial protonophore reverses diabetes and protonophore reverses diabetes and steatohepatitis in rats. *Science* **347**, 1253–1256
47. Kharroubi, A. T., Masterson, T. M., Aldaghlas, T. A., Kennedy, K. A., and Kelleher, J. K. (1992) Isotopomer spectral analysis of triglyceride fatty acid synthesis in 3T3-L1 cells. *Am J Physiol Endocrinol Metab* **263**, E667–E675
48. Cadenas, S. (2018) ROS and redox signaling in myocardial ischemia-reperfusion injury and cardioprotection. *Free Radic. Biol. Med.* **117**, 76–89
49. Peoples, J. N., Saraf, A., Ghazal, N., Pham, T. T., and Kwong, J. Q. (2019) Mitochondrial dysfunction and oxidative stress in heart disease. *Exp. Mol. Med.* **51**, 1–13
50. Weissman, D., and Maack, C. (2021) Redox signaling in heart failure and therapeutic implications. *Free Radic. Biol. Med.* **171**, 345–364
51. Chouchani, E. T., Pell, V. R., James, A. M., Work, L. M., Saeb-Parsy, K., Frezza, C., *et al.* (2016) A unifying mechanism for mitochondrial superoxide production during ischemia-reperfusion injury. *Cell Metab.* **23**, 254–263
52. Murphy, M. P. (2009) How mitochondria produce reactive oxygen species. *Biochem. J.* **417**, 1–13

53. Murphy, E., and Steenbergen, C. (2021) Regulation of mitochondrial Ca2+ uptake. *Annu. Rev. Physiol.* **83**, 107–126
54. Finkel, T., Menazza, S., Holmström, K. M., Parks, R. J., Liu, J., Sun, J., *et al.* (2015) The ins and outs of mitochondrial calcium. *Circ. Res.* https://doi.org/10.1161/CIRCRESAHA.116.305484
55. Bernardi, P. (2013) The mitochondrial permeability transition pore: a mystery solved? *Front. Physiol.* https://doi.org/10.3389/fphys.2013.00095
56. Reynolds, I. J., and Hastings, T. G. (1995) Glutamate induces the production of reactive oxygen species in cultured forebrain neurons following NMDA receptor activation. *J. Neurosci.* **15**, 3318–3327
57. Brennan, J. P., Southworth, R., Medina, R. A., Davidson, S. M., Duchen, M. R., and Shattock, M. J. (2006) Mitochondrial uncoupling, with low concentration FCCP, induces ROS-dependent cardioprotection independent of KATP channel activation. *Cardiovasc. Res.* **72**, 313–321
58. Minners, J., Van Den Bos, E. J., Yellon, D. M., Schwalb, H., Opie, L. H., and Sack, M. N. (2000) Dinitrophenol, cyclosporin A, and trimetazidine modulate preconditioning in the isolated rat heart: support for a mitochondrial role in cardioprotection. *Cardiovasc. Res.* **47**, 68–73
59. Hoerter, J., Gonzalez-Barroso, M. D. M., Couplan, E., Mateo, P., Gelly, C., Cassard-Doulcier, A. M., *et al.* (2004) Mitochondrial uncoupling protein 1 expressed in the heart of transgenic mice protects against ischemic-reperfusion damage. *Circulation* **110**, 528–533
60. Leak, M. H.+., Ambre, T., Bertholet, M., and Kirichok, Y. (2021) *Annu. Rev. Physiol.* https://doi.org/10.1146/annurev-physiol-021119
61. Harper, J. A., Dickinson, K., and Brand, M. D. (2001) Mitochondrial uncoupling as a target for drug development for the treatment of obesity. *Obes. Rev.* **2**, 255–265
62. Grundlingh, J., Dargan, P. I., El-Zanfaly, M., and Wood, D. M. (2011) 2,4-Dinitrophenol (DNP): a weight loss agent with significant acute toxicity and risk of death. *J. Med. Toxicol.* **7**, 205
63. Abulizi, A., Perry, R. J., Camporez, J. P. G., Jurczak, M. J., Petersen, K. F., Aspichueta, P., *et al.* (2017) A controlled-release mitochondrial protonophore reverses hypertriglyceridemia, nonalcoholic steatohepatitis, and diabetes in lipodystrophic mice. *FASEB J.* **31**, 2916–2924
64. Alexopoulos, S. J., Chen, S. Y., Brandon, A. E., Salamoun, J. M., Byrne, F. L., Garcia, C. J., *et al.* (2020) Mitochondrial uncoupler BAM15 reverses diet-induced obesity and insulin resistance in mice. *Nat. Commun.* **11**. https://doi.org/10.1038/S41467-020-16298-2
65. Voronova, V., Sokolov, V., Morias, Y., Boezelman, M. J., Wågberg, M., Henricsson, M., *et al.* (2022) Evaluation of therapeutic strategies targeting BCAA catabolism using a systems pharmacology model. *Front. Pharmacol.* **13**, 993422
66. Meyer, L. F., Rajadhyaksha, P. M., and Shah, D. K. (2022) Physiologically-based pharmacokinetic model for 2,4-dinitrophenol. *J. Pharmacokinet. Pharmacodynamics* **49**, 325–336
67. Roth Flach, R. J., Bollinger, E., Reyes, A. R., Laforest, B., Kormos, B. L., Liu, S., *et al.* (2023) Small molecule branched-chain ketoacid dehydrogenase kinase (BDK) inhibitors with opposing effects on BDK protein levels. *Nat. Commun.* **14**, 1–14
68. Liu, S., Kormos, B. L., Knafels, J. D., Sahasrabudhe, P. V., Rosado, A., Sommese, R. F., *et al.* (2023) Structural studies identify angiotensin II receptor blocker-like compounds as branched-chain ketoacid dehydrogenase kinase inhibitors. *J. Biol. Chem.* **299**, 102959
69. Nishi, K., Yoshii, A., Abell, L., Zhou, B., Frausto, R., Ritterhoff, J., *et al.* (2023) Branched-chain keto acids inhibit mitochondrial pyruvate carrier and suppress gluconeogenesis in hepatocytes. *Cell Rep.* **42**. https://doi.org/10.1016/J.CELREP.2023.112641
70. Hue, L., and Taegtmeyer, H. (2009) The Randle cycle revisited: a new head for an old hat. *Am. J. Physiol. Endocrinol. Metab.* https://doi.org/10.1152/ajpendo.00093.2009
71. Chen, M. J., Dixon, J. E., and Manning, G. (2017) Genomics and evolution of protein phosphatases. *Sci. Signal.* **10**, eaag1796
72. Joshi, M. A., Jeoung, N. H., Obayashi, M., Hattab, E. M., Brocken, E. G., Liechty, E. A., *et al.* (2006) Impaired growth and neurological abnormalities in branched-chain alpha-keto acid dehydrogenase kinase-deficient mice. *Biochem. J.* **400**, 153–162
73. Rubio, M., Avitabile, D., Fischer, K., Emmanuel, G., Gude, N., Miyamoto, S., *et al.* (2009) Cardioprotective stimuli mediate phosphoinositide 3-kinase and phosphoinositide dependent kinase 1 nuclear accumulation in cardiomyocytes. *J. Mol. Cell Cardiol.* **47**, 96–103
74. Li, S., Yokota, T., Wang, P., ten Hoeve, J., Ma, F., Le, T. M., *et al.* (2022) Cardiomyocytes disrupt pyrimidine biosynthesis in nonmyocytes to regulate heart repair. *J. Clin. Invest.* **132**. https://doi.org/10.1172/JCI149711
75. Acín-Pérez, R., Montales, K. P., Nguyen, K. B., Brownstein, A. J., Stiles, L., and Divakaruni, A. S. (2023) Isolation of mitochondria from mouse tissues for functional analysis. *Methods Mol. Biol. (Clifton, N.J.)* **2675**, 77–96
76. Divakaruni, A. S., Paradyse, A., Ferrick, D. A., Murphy, A. N., and Jastroch, M. (2014) Analysis and interpretation of microplate-based oxygen consumption and pH data. *Methods Enzymol.* **547**, 309–354
77. Yang, K., Doan, M. T., Stiles, L., and Divakaruni, A. S. (2021) Measuring CPT-1-mediated respiration in permeabilized cells and isolated mitochondria. *STAR Protoc.* **2**. https://doi.org/10.1016/J.XPRO.2021.100687
78. Rogers, G. W., Brand, M. D., Petrosyan, S., Ashok, D., Elorza, A. A., Ferrick, D. A., *et al.* (2011) High throughput microplate respiratory measurements using minimal quantities of isolated mitochondria. *PLoS One*. https://doi.org/10.1371/journal.pone.0021746
79. Orr, A. L., Ashok, D., Sarantos, M. R., Ng, R., Shi, T., Gerencser, A. A., *et al.* (2014) Novel inhibitors of mitochondrial sn-glycerol 3-phosphate dehydrogenase. *PLoS One* **9**, e89938
80. Bertholet, A. M. (2021) The use of the patch-clamp technique to study the thermogenic capacity of mitochondria. *J. Vis. Exp.* **2021**. https://doi.org/10.3791/62618
81. Vacanti, N. M., Divakaruni, A. S., Green, C. R., Parker, S. J., Henry, R. R., Ciaraldi, T. P., *et al.* (2014) Regulation of substrate utilization by the mitochondrial pyruvate carrier. *Mol. Cell*. https://doi.org/10.1016/j.molcel.2014.09.024
82. Cordes, T., and Metallo, C. M. (2019) Quantifying intermediary metabolism and lipogenesis in cultured mammalian cells using stable isotope tracing and mass spectrometry. *Methods Mol. Biol.* **1978**, 219–241
83. Trefely, S., Ashwell, P., and Snyder, N. W. (2016) FluxFix: automatic isotopologue normalization for metabolic tracer analysis. *BMC Bioinform.* https://doi.org/10.1186/s12859-016-1360-7
84. Chen, M., Gao, C., Yu, J., Ren, S., Wang, M., Wynn, R. M., *et al.* (2019) Therapeutic effect of targeting branched-chain amino acid catabolic flux in pressure-overload induced heart failure. *J. Am. Heart Assoc.* **8**. https://doi.org/10.1161/JAHA.118.011625